iScience

CellPress
OPEN ACCESS

Article

GPC3-mediated metabolic rewiring of diabetic mesenchymal stromal cells enhances their cardioprotective functions via PKM2 activation

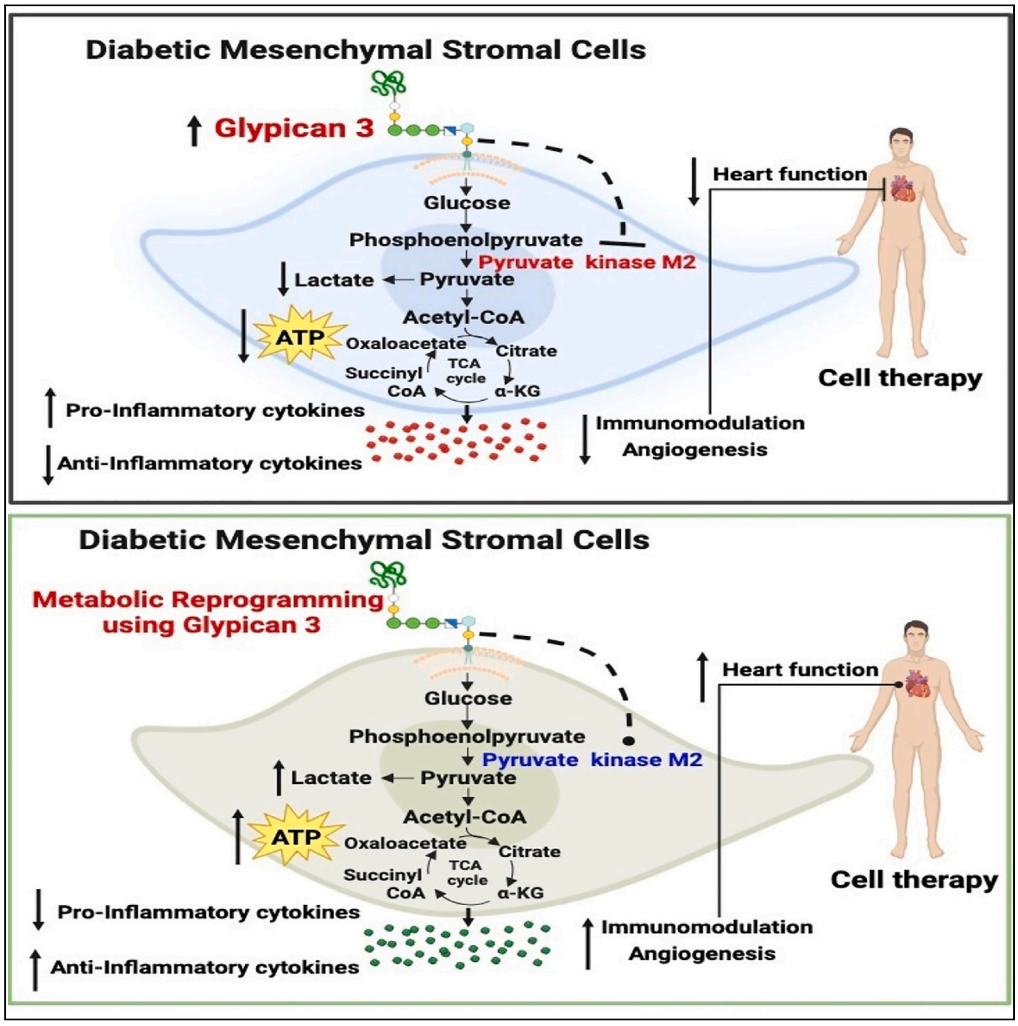

Darukeshwara Joladarashi, Charan Thej, Vandana Mallaredy, ..., Cindy Benedict, Walter J. Koch, Raj Kishore

raj.kishore@temple.edu

Highlights

Diabetes impairs mesenchymal stem cell (MSC) cardiac reparative functions

Diabetic-MSC shows a highly upregulated expression of GPC3

Diabetic MSC dysfunction involves GPC3 induced metabolic alterations

GPC knockdown improves MSC metabolisms and cardiac reparative functions

Joladarashi et al., iScience 27, 111021
October 18, 2024
https://doi.org/10.1016/j.isci.2024.111021

iScience

CellPress
OPEN ACCESS

Article

GPC3-mediated metabolic rewiring of diabetic mesenchymal stromal cells enhances their cardioprotective functions via PKM2 activation

Darukeshwara Joladarashi,[1] Charan Thej,[1] Vandana Mallaredy,[1] Ajit Magadum,[1] Maria Cimini,[1] Carolina Gonzalez,[1] May Truongcao,[1] Joseph T. Nigro,[2] Manveen K. Sethi,[2] Andrew A. Gibb,[3] Cindy Benedict,[1] Walter J. Koch,[4] and Raj Kishore[1,5,6,*]

SUMMARY

Mesenchymal stromal cells (MSC) are promising stem cell therapy for treating cardiovascular and other degenerative diseases. Diabetes affects the functional capability of MSC and impedes cell-based therapy. Despite numerous studies, the impact of diabetes on MSC myocardial reparative activity, metabolic fingerprint, and the mechanism of dysfunction remains inadequately perceived. We demonstrated that the transplantation of diabetic-MSC (db/db-MSC) into the ischemic myocardium of mice does not confer cardiac benefit post-MI. Metabolomic studies identified defective energy metabolism in db/db-MSC. Furthermore, we found that glypican-3 (GPC3), a heparan sulfate proteoglycan, is highly upregulated in db/db-MSC and is involved in metabolic alterations in db/db-MSC via pyruvate kinase M2 (PKM2) activation. GPC3-knockdown reprogrammed-db/db-MSC restored their energy metabolic rates, immunomodulation, angiogenesis, and cardiac reparative activities. Together, these data indicate that GPC3-metabolic reprogramming in diabetic MSC may represent a strategy to enhance MSC-based therapeutics for myocardial repair in diabetic patients.

INTRODUCTION

Cardiovascular diseases frequently affect patients with diabetes, imposing a significant public health burden due to high mortality rates and disability.[1–3] In the absence of effective endogenous repair mechanisms after ischemic injury, cell-based therapies have emerged as a potential therapeutic approach for ischemic myocardial repair.[4–6] Mesenchymal stromal cells, also known as "medicinal signaling cells" (MSCs), are favored in cell-based therapy because they possess an immune-privileged phenotype, are easy to isolate, and exhibit paracrine activity.[7–9] Mounting evidence suggests that MSC harvested from diabetic donors display impaired functionality, both *in vitro* and *in vivo*.[10,11] Diabetes impairs the MSC secretome related to its immunomodulation properties and angiogenic potential, thereby reducing its clinical efficacy.[12] Although preclinical and clinical studies have demonstrated the advantages of using autologous and allogeneic MSC in treating heart failure and diabetes, the survival of transplanted MSC and their secretion of paracrine molecules are severely impaired due to increased reactive oxygen species (ROS) production under hyperglycemic conditions and myocardial infarction, which could trigger apoptosis.[13] However, the mechanisms of diabetes-induced MSC dysfunction and their diminished tissue reparative properties are not well understood.

Metabolic abnormalities play a significant role in the decline of stem cell function associated with disease.[14] Emerging evidence indicates that the metabolic characteristics of MSCs, including their capacity for both glycolysis and oxidative phosphorylation, influence their functional roles.[15,16] Previous studies have revealed that human MSCs from aged donors and those with age-related atherosclerosis exhibit altered metabolism and diminished mitochondrial function.[17] In particular, RNA sequencing profiles of bone marrow MSCs from old rats compared to young rats show significant transcriptome changes, with metabolism-related processes affected, including glucose uptake, lactate secretion, Adenosine triphosphate (ATP) production, and extracellular acidification rates.[18] Despite this knowledge, the precise impact of diabetes on MSC metabolic activity and the underlying molecular mechanisms that impair their reparative functions are seldom studied.

Glypican-3 (GPC3) is a heparan sulfate proteoglycan (HSPG) found on mammalian cell surfaces and anchored to the plasma membrane via a glycosylphosphatidylinositol (GPI) protein.[19–21] GPC3 regulates cell migration, proliferation, apoptosis, and differentiation by modulating

[1]Aging and Cardiovascular Discovery Center, Lewis Katz School of Medicine, Temple University, Philadelphia, PA 19140, USA
[2]Center for Biomedical Mass Spectrometry, Department of Biochemistry & Cell Biology, Boston University Chobanian and Avedisian School of Medicine, Boston, MA, USA
[3]Center for Cardiometabolic Science, Christina Lee Brown Envirome Institute, University of Louisville, 580 South Preston Street, Louisville, KY, USA
[4]Department of Surgery, Duke University School of Medicine, Durham, NC 27710, USA
[5]Department of Cardiovascular Sciences, Lewis Katz School of Medicine, Temple University, Philadelphia, PA 19140, USA
[6]Lead contact
*Correspondence: raj.kishore@temple.edu
https://doi.org/10.1016/j.isci.2024.111021

various growth factors and signal pathways.[22,23] GPC3 acts as a co-receptor for cell-surface receptors in several signaling pathways, including Hedgehog (Hh), Wnt, bone morphogenetic protein (BMP), and fibroblast growth factor (FGF) signaling.[24–26] GPC3 has been reported as a tumor biomarker in hepatomas.[27,28] GPC3 has been reported to trigger the transformation of mesenchymal to epithelial cells in human breast cancer cells.[29] Recently, Szoor et al., showed that genetically modified MSC expressing GPC3-ENG with costimulatory molecules have redirected T cells toward GPC3+ tumor cells and exhibited significant antitumor activity.[30] However, the effect of GPC3 on the functions and metabolic activity of MSC remains largely unexplored.

Our study demonstrates that diabetic-MSC does not cf. cardiac benefit post-myocardial infarction (MI) and is devoid of metabolic demands. Interestingly, GPC3 is highly expressed in diabetic-MSC and GPC3 suppression reprogrammed-db/db-MSC and restored their metabolic rates. Mechanistically, we have discovered that GPC3 interacts with pyruvate kinase M2 (PKM2), which subsequently increases the glycolysis, oxidative phosphorylation, and ATP production rate. Furthermore, GPC3 metabolic reprogrammed-db/db-MSC confers cardiac benefit post-MI. Together, our findings indicate that metabolic reprogrammed-db/db-MSC could potentially be used to restore the metabolic state and functions of db/db-MSC in cell therapy applications.

RESULTS

Diabetic MSC are deficient in post-MI cardiac repair activity

Mounting evidence suggests diabetes-induced MSC functional impairment *in vitro*.[10,11] However, the effect of diabetes on the reparative capacity of MSC on post-MI cardiac repair and functions is seldom studied. To study the cardiac reparative function of diabetic-MSC, MSC were isolated from the bone marrow of db/+ non-diabetic (WT-MSC) and db/db diabetic mice (db/db-MSC). Cell surface marker analyses by flow cytometry revealed that the cells were positive for CD90 and CD105 (MSC markers) and negative for hematopoietic cell lineage-specific antigens, such as CD45 (Figure S1A). There were no differences in the expression of MSC markers between WT-MSC and db/db-MSC (Figure S1A). Furthermore, to evaluate its multipotent lineage differentiation characteristics, we differentiated the cells into adipogenic, osteogenic, and chondrogenic cell lineage as assessed by staining with Oil Red O, Alizarin Red, and Alcian blue, respectively (Figures S1B–S1D). The potential for differentiation was observed to be decreased in db/db-MSC when compared to WT-MSC (Figures S1B–S1D).

To investigate the impact of db/db-MSC therapy on cardiac function, we used a WT mouse model of MI. Following left anterior descending artery (LAD) ligation, WT-MSC or db/db-MSC (5×10^5) were immediately transplanted into the peri-infarct area of the hearts. Echocardiography was performed on days 0, 7, and 14 post-MI to measure cardiac function. Left ventricular (LV) ejection fraction (EF) and fractional shortening (FS) were significantly improved in mice treated with WT-MSC (Figures 1A and 1B). Furthermore, LV end-diastolic volume, LV end-systolic volume, LV end-diastolic diameter, and LV end-systolic diameter were significantly improved in mice treated with WT-MSC (Figures 1C–1F). Conversely, no cardiac function improvements were observed when mice were treated with db/db-MSC (Figures 1A–1H). These findings suggest that db/db-MSC loses cardiac function beneficial effects in ischemic hearts.

Diabetes decreases the energy status of MSC

MSC functions are determined by their metabolic commitment.[14] To confirm *in vivo* functional impairment of diabetic MSCs may represent an alteration in their metabolic activity, we evaluated their metabolic activity using a seahorse metabolic assay. We determined the extracellular acidification rate (ECAR) as an indicator of glycolysis and oxygen consumption rate (OCR) to quantify mitochondrial respiration (OXPHOS). We found major differences in ECAR between db/db-MSC and WT-MSC (Figure 2A). Compared to WT-MSC, db/db-MSC exhibited a significantly lower glycolysis rate, glycolytic capacity, and glycolytic reserve (Figures 2B–2D). On the other hand, a striking difference between the WT-MSC and db/db-MSC was observed in OCR, which was significantly decreased in db/db-MSC (Figure 2E). Quantification of these results confirmed that the basal and maximal respiration capacity of the db/db-MSC was decreased (Figures 2F and 2G). ATP formation was also decreased in db/db-MSC compared to WT-MSC (Figure 2H).

Next, ^{13}C glucose tracing metabolomics profiling of WT-MSC and db/db-MSC exhibited a significant reduction in the concentration of metabolic intermediates related to glycolysis and tricarboxylic acid cycle in the db/db-MSC group (Figure 2I). The differential metabolites among the WT-MSC and db/db-MSC were further analyzed on the Koto encyclopedia of genes and genomes (KEGG) pathways, to identify the top 25 altered metabolic pathways (Figure 2J). The metabolic alterations were associated with glycolysis and the tricarboxylic acid (TCA) cycle, consistent with the reduced ECAR and OCR. Together, this metabolic analysis showed that diabetic MSC showed diminished energy metabolism.

Glypican 3 expression is highly upregulated in db/db-MSC

To understand the molecular mechanism of altered metabolism and dysfunctional activities of diabetic MSC, we determined the expression of heparan sulfate proteoglycans (HSPGs) in db/db-MSC. Biosynthesis of HSPGs in the cell is essential for development and homeostasis and has been critically implicated in various pathophysiological phenomena.[31,32] HSPGs and HS disaccharide chains are synthesized by the cooperation of multiple biosynthetic enzymes in the Golgi and include genes that code for both HSPGs and disaccharide chains. RT-PCR analysis showed highly upregulated mRNA expression of both HSPGs and disaccharide chains in db/db-MSC compared to WT-MSC (Figure 3A; S2A-2B). Concordantly, human MSC treated with high glucose (25 mM) to mimic diabetes-related hyperglycemia showed similarly increased mRNA expression of both HSPGs and disaccharide chains compared with MSC from the normoglycemic condition (Figures S2C–S2E).

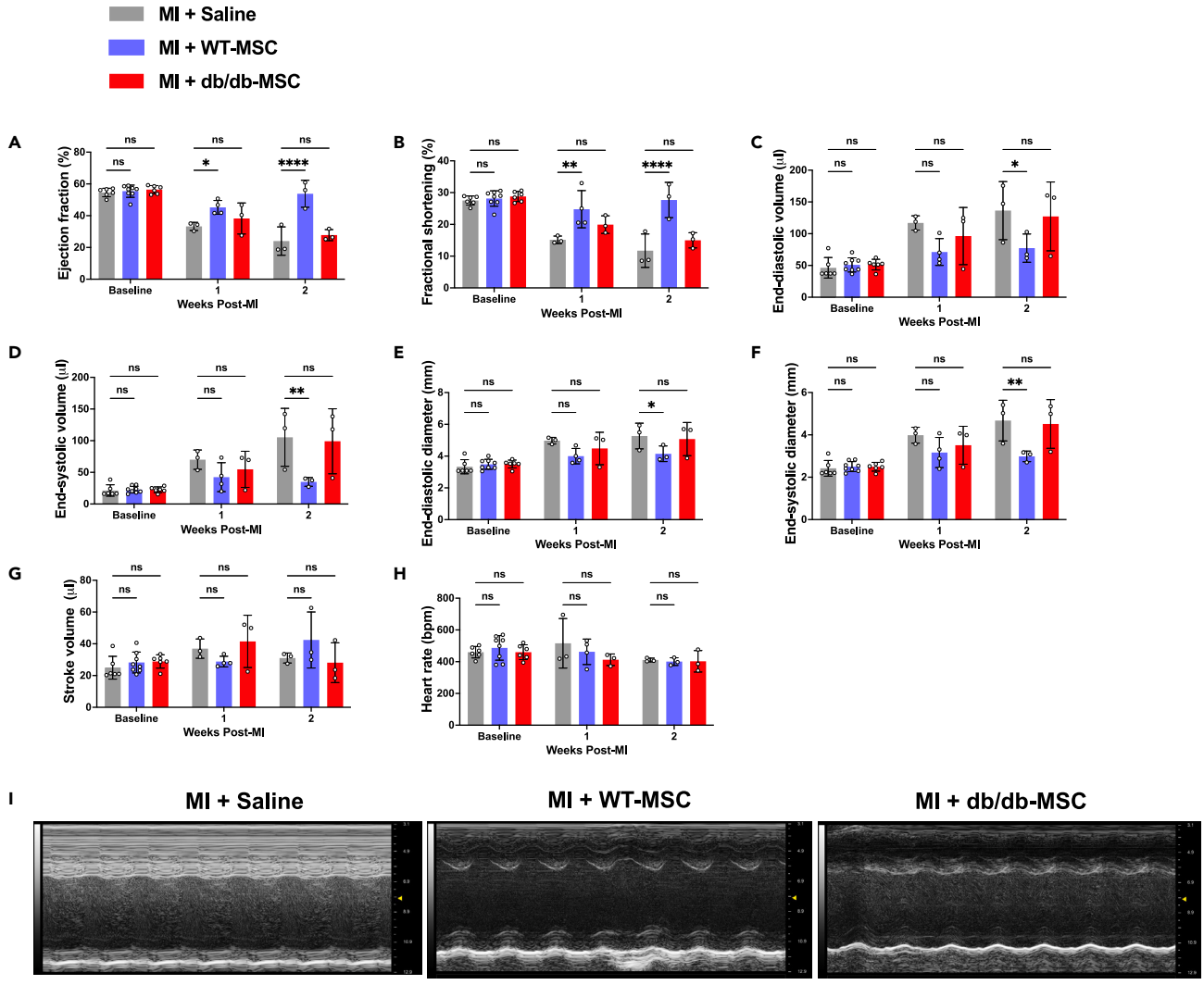

Figure 1. Diabetic MSC does not improve cardiac functions post-MI

(A–H) Baseline echocardiography measurements were conducted on C57BL/6J mice before they underwent left anterior descending coronary artery ligation followed by saline, WT-MSC, or db/db-MSC treatment. (A) Ejection fraction, (B) fractional shortening, (C) end-diastolic volume, (D) end-systolic volume, (E) end-diastolic diameter, (F) end-systolic diameter, (G) stroke volume, and (H) heart rate was assessed up to 2 weeks post-MI (n = 3–8/group).

(I) Representative echocardiographic images (M-mode) from saline, WT-MSC, and db/db-MSC-treated MI mouse hearts at 2 weeks. Data are displayed as mean ± SEM. Two-way ANOVA, in conjunction with Tukey's multiple comparisons test. *$p < 0.05$, **$p < 0.01$, ****$p < 0.0001$.

Glypican-3 (GPC3) expression was the most upregulated HSPG mRNA in diabetic MSCs (Figure 3A) (and its analog GPC5 in human MSCs treated with high glucose)[33,34] (Figure S2C) compared to all other HSPGs. We chose GPC3 for further study. Western blotting and immunofluorescence confirmed increased GPC3 protein expression in db/db-MSC (Figures 3B and 3C).

Restoration of impaired immunomodulation, angiogenesis, and energy metabolism by metabolic rewiring through GPC3 knockdown in db/db-MSC

Diabetes impairs MSC function *in-vitro* and has been well studied.[35] Our results showed that diabetes has a deleterious effect on MSC metabolic activities and *in-vivo* cardiac functions. Previous studies demonstrated that metabolic reprogramming of MSC promoted self-renewal capacities and enhanced the functions of MSC.[36–38] Next, we tested whether metabolic reprogramming of db/db-MSC by inhibiting GPC3 could reverse diabetes-induced dysfunction and diminished energy metabolism. We created a stable GPC3 knockdown-db/db-MSC cell line using GPC3 siRNA (Figure 4A), and GPC3 knockdown in db/db-MSC was confirmed by western blot (Figure 4B). Diabetes is known to decrease the proliferation of MSC.[39] Interestingly, GPC3 knockdown-db/db-MSC restored the diabetes-induced impairment in MSC proliferation (Figure 4C).

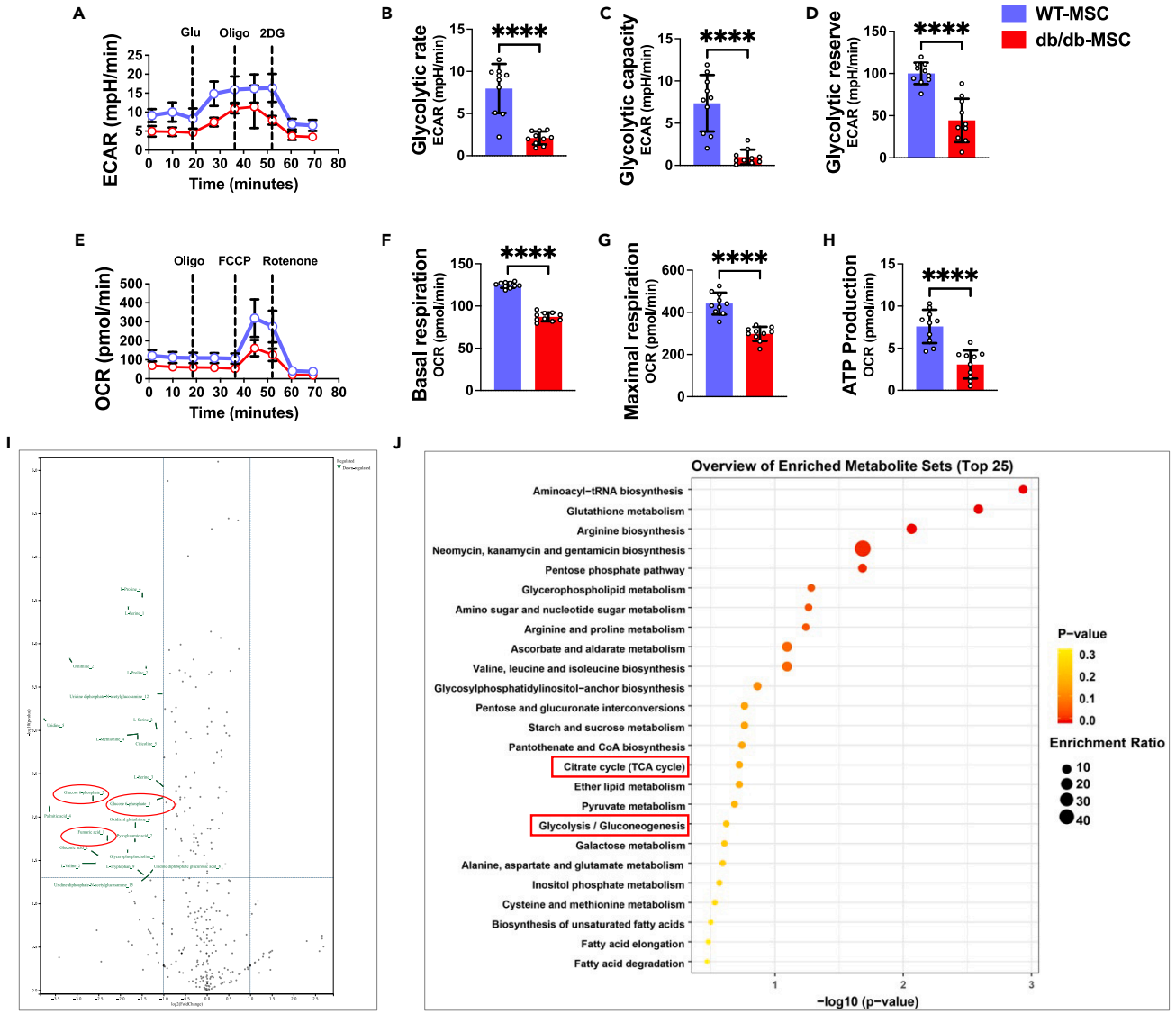

Figure 2. Diabetes alters the metabolic profile of MSC

(A–H) The metabolic profile of db/db-MSC was evaluated by measuring the extracellular acidification rate (ECAR) for glycolysis and the oxygen consumption rates (OCR) for oxidative phosphorylation using the Agilent Seahorse XF Cell Energy Phenotype Test. (A) ECAR, (B) quantification of glycolytic rate, (C) glycolytic capacity, and (D) glycolytic reserve. (E) OCR (F) quantification of basal respiration, (G) maximal respiration, and (H) ATP production in db/db-MSC. (A–H) Data are representative of two independent experiments with ten technical repeats per experiment. Data are expressed as mean ± SEM. Unpaired Student's t test was applied. ****$p < 0.0001$.

(I) Metabolomic analysis in db/db-MSC: Volcano plot of metabolites altered in db/db-MSC compared to WT-MSC.

(J) The dot blot shows that metabolic pathways are significantly altered in db/db-MSC compared to WT-MSC.

The diabetic MSC is reported to secrete less immunomodulatory cytokines and more pro-inflammatory cytokines.[12,40] To test the effect of GPC3 knockdown on the paracrine secretome of db/db-MSC under inflammatory stimuli, cells at 80% confluence were treated with 10 ng/mL interferon gamma (IFN-γ) and 15 ng/mL tumor necrosis factor α (TNF-α) (primed MSCs) or not (resting MSCs) for 48 h and secretome was collected. We quantified a comprehensive panel of 40 pro-inflammatory factors in the secretome. We found that, overall, control siRNA-db/db-MSC secreted higher levels of proinflammatory cytokines such as interleukin 6 (IL-6), monokine induced by gamma interferon/ Chemokine ligand 9 (MIG/CXCL9), and Lipopolysaccharide-induced CXC chemokine (LIX) and decreased concentrations of anti-inflammatory cytokines compared to WT-MSC (Figures 4D–4H). Interestingly, GPC3 knockdown-db/db-MSC secreted low levels of proinflammatory cytokines and increased concentrations of anti-inflammatory cytokines compared to control-siRNA-db/db-MSC under inflammatory stimuli (Figures 4D–4H). Activation of T cells and the resulting inflammatory responses after cardiac injury contribute to adverse remodeling and

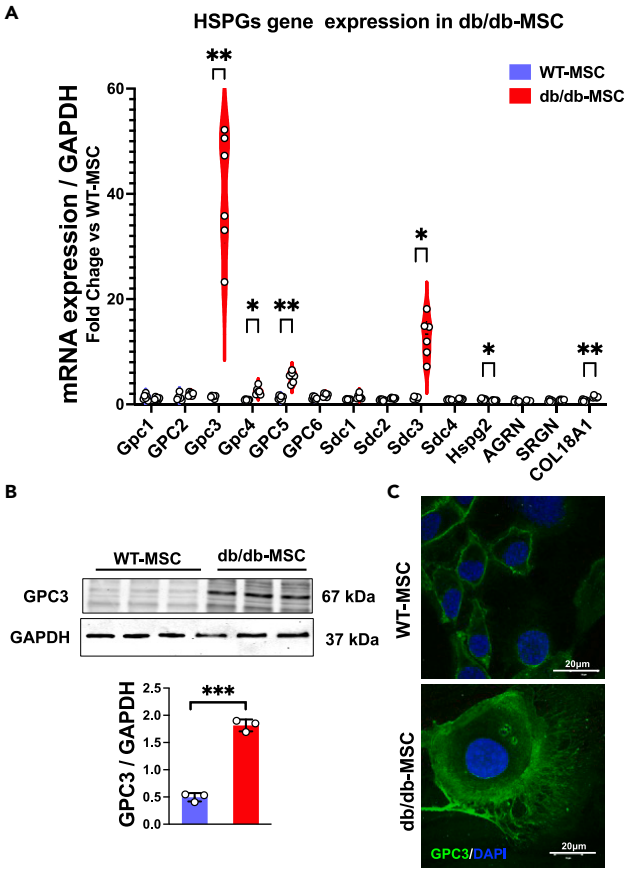

Figure 3. Heparan sulfate proteoglycan expression is altered in diabetic MSC

(A) SYBR Green real-time PCR analysis of heparan sulfate proteoglycans (HSPGs) genes in db/db-MSC and WT-MSC. Data normalized to GAPDH. $n = 6$; Data are displayed as mean ± SEM. Two-way ANOVA, in conjunction with Bonferroni's multiple comparisons test. $^{*}p < 0.05$, $^{**}p < 0.01$.

(B) Western blot analysis and quantification of glypican 3 (GPC3) expression in WT-MSC and db/db-MSC. Data was normalized to GAPDH. $n = 3$; Data are displayed as mean ± SEM and an unpaired Student's t test was applied. $^{***}p < 0.001$.

(C) Immunofluorescence staining to determine GPC3 expression (green) and nuclei, DAPI (blue) in WT-MSC and db/db-MSC. Scale bars: 20 μm.

development of heart failure.[41] MSCs have been shown to suppress T cell activation.[42] Therefore, we examined the ability of GPC3 knockdown db/db-MSC on T cell proliferation, which was either unstimulated or pre-stimulated with CD3/CD28. The GPC3 knockdown-db/db-MSC cocultured with activated T cells showed decreased T cell proliferation compared to control siRNA-db/db-MSC. (Figure 4I). The immunosuppressive property of MSC was calculated by their potential to inhibit T cell proliferation. These results showed that GPC3 knockdown in db/db-MSC reverses the immunomodulatory effects of db/db-MSC that are diminished in db/db-MSC and can maintain the ability to block T cell proliferation and cytokine production.

Neovascularization/angiogenesis is crucial for cardiac repair post-MI.[43] Therefore, we performed tube formation assays to measure endothelial angiogenic activity in response to GPC3 knockdown-db/db-MSC. We found that tube formation activity was significantly diminished by control siRNA-db/db-MSC (Figure 4J). Interestingly, GPC3 knockdown-db/db-MSC significantly increased the human umbilical vein endothelial cells (HUVEC) tube formation compared to control siRNA-db/db-MSC (Figure 4J). The above functional analysis revealed that GPC3 knockdown in db/db-MSC has a positive impact on regulating immunomodulation and enhancing angiogenic activity.

We have shown that db/db-MSC have defective metabolic activity and *in vivo* functional impairments. We checked their metabolic profile since GPC3 knockdown in db/db-MSC has shown *in vitro* functional improvement. ECAR data showed that compared to control siRNA-db/db-MSC, GPC3 knockdown-db/db-MSC exhibited a significantly increased rate of glycolysis, glycolytic capacity, and glycolytic reserve (Figures 5A–5D). OCR results indicated that GPC3 knockdown-db/db-MSC shows significantly enhanced basal respiration, maximum respiration rate, and increased ATP production compared to control siRNA-db/db-MSC (Figures 5E–5H). Furthermore, metabolomics results showed several altered metabolites of glycolysis and TCA cycle in GPC3 knockdown-db/db-MSC (Figures 5I and 5J). Interestingly, pyruvic acid, lactic acid (glycolysis metabolites), and oxo-glutaric acid (TCA cycle metabolites) were significantly decreased in control-siRNA-db/db-MSC and restored in GPC3 knockdown-db/db-MSC (Figure 5K). Thus, GPC3 knockdown in diabetic MSC showed increased glycolytic

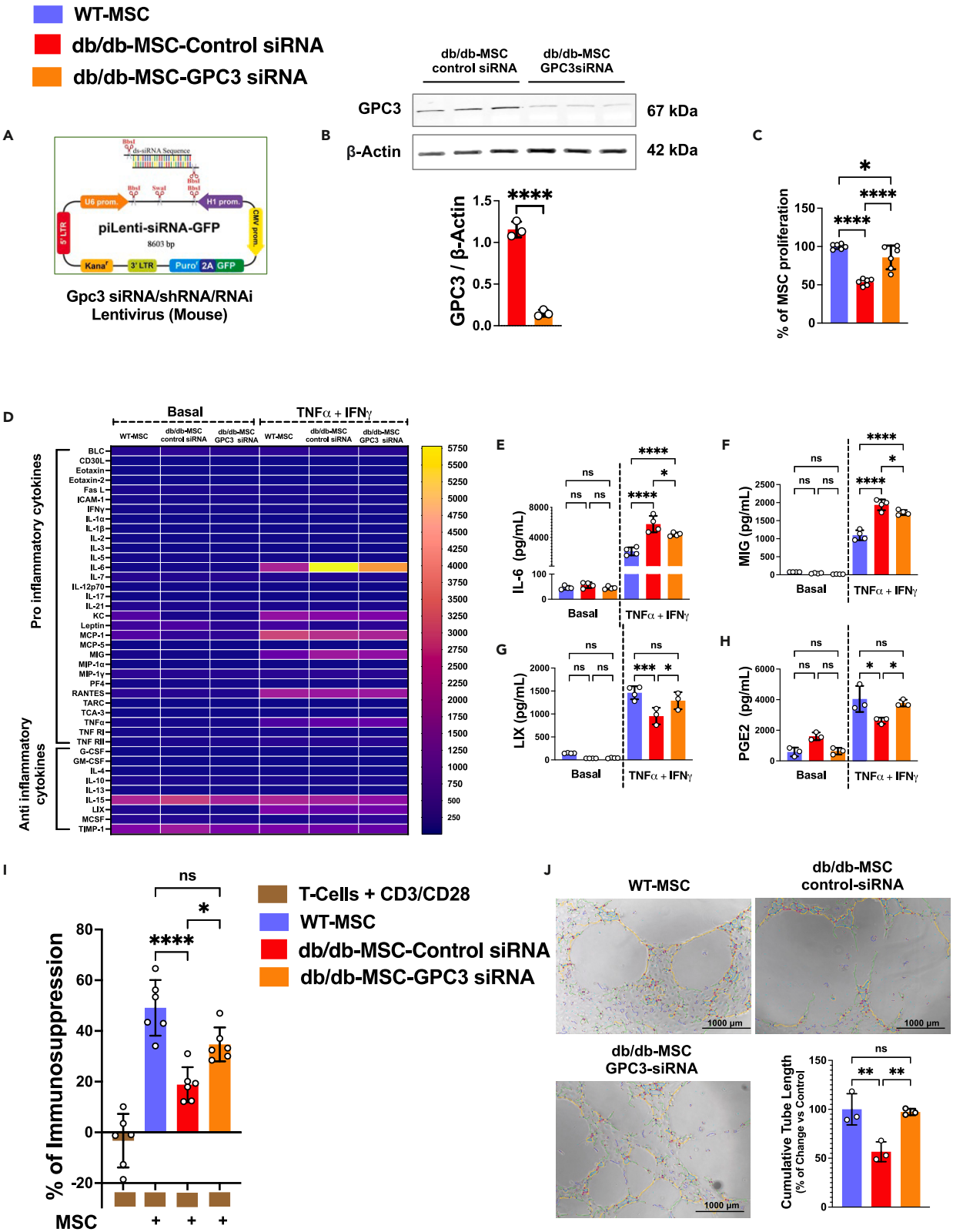
WT-MSC
db/db-MSC-Control siRNA
db/db-MSC-GPC3 siRNA
A
Gpc3 siRNA/shRNA/RNAi
Lentivirus (Mouse)
piLenti-siRNA-GFP
8603 bp
B
db/db-MSC control siRNA
db/db-MSC GPC3siRNA
GPC3
67 kDa
β-Actin
42 kDa
GPC3 / β-Actin
C
% of MSC proliferation
D
Basal
TNFα + IFNγ
Pro inflammatory cytokines
Anti inflammatory cytokines
E
IL-6 (pg/mL)
F
MIG (pg/mL)
G
LIX (pg/mL)
H
PGE2 (pg/mL)
I
% of Immunosuppression
MSC
T-Cells + CD3/CD28
WT-MSC
db/db-MSC-Control siRNA
db/db-MSC-GPC3 siRNA
J
WT-MSC
db/db-MSC control-siRNA
db/db-MSC GPC3-siRNA
1000 μm
Cumulative Tube Length (% of Change vs Control)

Figure 4. GPC3 knockdown restores impaired immunomodulation and angiogenesis activities of db/db-MSC

(A) Sequence map of GPC3-specific piLenti-siRNA.

(B) Western blot analysis and quantification of GPC3 expressions in db/db-MSC-control siRNA and db/db-MSC-GPC3 siRNA. Data was normalized to β-actin. $n = 3$; Data are displayed as mean ± SEM and an unpaired Student's t test was applied. ****$p < 0.0001$.

(C) Quantification of db/db-MSC-GPC3 siRNA proliferation measured using the BrdU kit. $n = 6$; Data are displayed as mean ± and an unpaired Student's t test was applied. *p < 0.05, ****$p < 0.0001$.

(D) Heatmap showing the concentration of the differentially secreted cytokine (pg/mL) in supernatants collected from db/db-MSC-GPC3 siRNA with TNF-α and IFN-γ stimulation.

(E–H) Significantly expressed cytokines in supernatants collected from db/db-MSC-GPC3 siRNA with TNF-α and IFN-γ stimulation. $n = 3$–4; Data are displayed as mean ± SEM. Significance was determined by one-way ANOVA. *$p < 0.05$, ***$p < 0.001$, ****$p < 0.0001$.

(I) The immunosuppressive ability of GPC3 knockdown db/db-MSC co-cultured with activated T cells. The T cell proliferation was measured using the BrdU kit, and the immunosuppressive property of MSC was calculated by their potential to inhibit T cell proliferation. $n = 6$; Data are displayed as mean ± SEM. Significance was determined by one-way ANOVA. *$p < 0.05$, ****$p < 0.0001$.

(J) Representative photomicrographs (1,000 μm) of tube formation in HUVEC in the presence of condition media collected from WT-MSC or db-db-MSC-control siRNA or db/db-MSC-GPC3 siRNA and quantification of relative quantification of tube length. $n = 3$; Data are displayed as mean ± SEM. Significance was determined by one-way ANOVA. **$p < 0.01$.

and oxidative phosphorylation activities. All these results demonstrated that metabolic rewiring of db/db-MSC by inhibiting GPC3 improves MSC immunomodulation, angiogenic potential, and energy metabolism state.

In parallel experiments, we also created a stable WT-MSC cell line overexpressing GPC3 using GPC3 lentivirus (Figure S3A), and GPC3 overexpression was confirmed by western blot (Figure S3B). GPC3-overexpressing-WT-MSC showed a significantly decreased proliferation compared to control lentivirus transfected-MSC (Figure S3C). Interestingly, under inflammatory stimuli, GPC3-overexpressing-WT-MSC secreted increased proinflammatory cytokines such as TNF-α, TNF-RI, and TNF-RII, and decreased anti-inflammatory cytokine PGE2 compared to control lentivirus transfected-MSC (Figures S3D–S3H). Further, GPC3-overexpressing WT-MSC showed decreased immunosuppression and angiogenesis activity (Figures S3I and S3J).

Since GPC3-overexpression negatively affects MSC functions, we next assessed its effect on MSC metabolic activity. The seahorse metabolic assay data showed that GPC3-overexpressing-MSC decreases the rate of glycolysis, basal respiration, and maximal respiration. There was no change in the glycolytic capacity, glycolytic reserve, and production of ATP (Figures S4A–S4H). Our ^{13}C glucose tracing metabolomics profiling showed differentially abundant metabolites of glycolysis and TCA cycle, but there were no significantly changed metabolites between the groups (data not shown). All these results illustrate that GPC3 overexpression induces MSC dysfunction and mild abnormal energy metabolism.

GPC3 binds to pyruvate kinase-M2

To further investigate the mechanism underlying the beneficial role of GPC3 knockdown in diabetic-MSC functions and metabolic state, we performed GPC3 pull-down and LC-MS/MS analysis to explore GPC3 binding to potential proteins in db/db-MSC. The Liquid chromatography-tandem mass spectrometry LC-MS/MS results differentially quantified 14 proteins interacting with GPC3 (Figure 6A). Among the 14 proteins, we have focused on pyruvate kinase (PK) because our metabolomics results have shown that GPC3 knockdown in db/db-MSC increased glycolysis and oxidative phosphorylation and PK is an important enzyme in controlling the rate-limiting step glycolysis.[44] To confirm the isomer for PK, we compared the peptide sequences for PKM1 and PKM2 from Uniports and further looked for the peptides distinctive for the isomer identification in our data; we found one peptide similar to PKM2 isomer and confirmed the peptide sequence by tandem LC-MS/MS spectra (Figure 6B). Further, we demonstrated the interaction of GPC3 with PKM2 by coimmunoprecipitation (coIP) (both GPC3 and PKM2 pull down) and western blot analysis using a PKM2 and GPC3-specific antibody (Figure 6C). Our confocal immunofluorescence analysis further confirmed the interaction of GPC3 with PKM2 (Figure 6E). Notably, enzyme-linked immunosorbent assay (ELISA) results showed increased PK activity in GPC3 knockdown-db/db-MSC compared to control-siRNA-db/db-MSC (Figure 6D). Together, our results showed that the GPC3 interacts with PKM2.

Intracardiac transplantation of GPC3 metabolic reprogrammed-db/db-MSC confers cardiac benefit post-MI

Our *in vitro* data indicates that db/db-MSCs with GPC3-metabolic reprogramming have positive effects on their immunomodulatory and angiogenic properties. The therapeutic efficacy of GPC3-metabolic reprogrammed db/db-MSC was evaluated in a mouse model of MI. Following LAD ligation, db/db-MSC-control-siRNA or db/db-MSC-GPC3-siRNA (5×10^5) were immediately transplanted into the peri-infarct area of the hearts. The left ventricular (LV) functions were analyzed using M-mode echocardiography at 0 (baseline), 7-, 14-, 21-, and 28-day post-MI and cell therapy. Percent ejection fraction (EF) and fractional shortening (FS) were similar at baseline (day 0) in all the groups. Strikingly, compared to db/db-MSC-control-siRNA, which showed no cardiac reparative activity, intramyocardial injection of GPC3-metabolic reprogrammed db/db-MSC significantly improved %EF (Figure 7A) and %FS (Figure 7B) at day 7, 14, 21, and 28-day post-MI. Analysis of LV end-diastolic volume, LV end-systolic volume, LV internal diameter during diastole (LVIDd), and systole (LVIDs) revealed a significant attenuation of LV dimension and volume with GPC3-metabolic reprogrammed db/db-MSC treatment (Figures S5A–S5D).

There were no significant differences in stroke volume, cardiac output, and LV mass between GPC3-metabolic reprogrammed db/db-MSC and db/db-MSC-control-siRNA (Figures S5E–S5G).

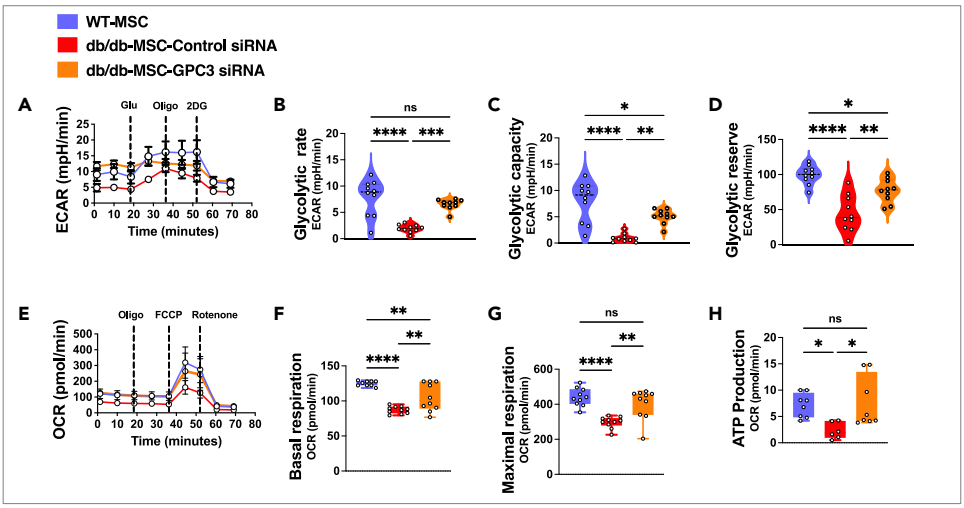

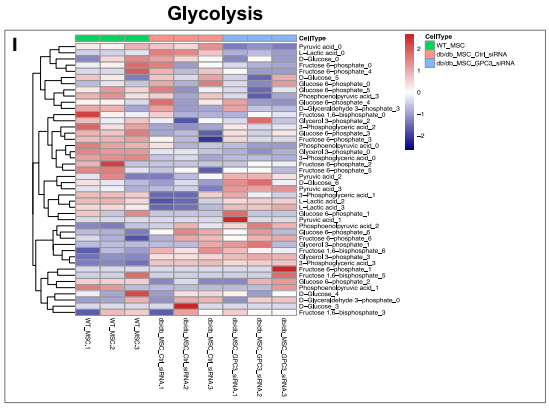

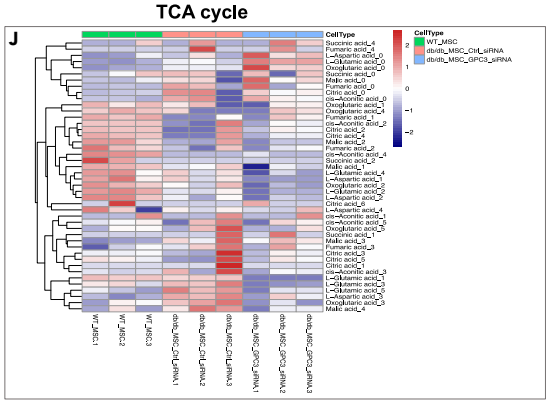

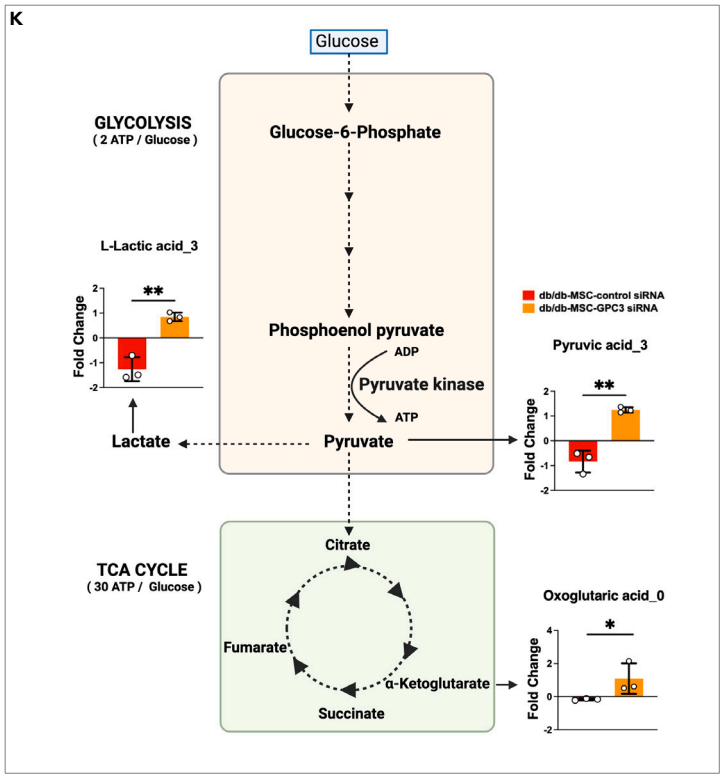

Figure 5. Metabolic indices of GPC3 knockdown db/db-MSC

(A–H) Seahorse metabolic analysis of WT-MSC, db-db-MSC-control siRNA, and db/db-MSC-GPC3 siRNA, showing (A) extracellular acidification rate (ECAR), (E) the oxygen consumption rates (OCR), and (B–D and E–H) quantification of metabolic readouts. Data are representative of two independent experiments with ten technical repeats per experiment. Data are expressed as mean ±SEM. Significance was determined by one-way ANOVA. *$p < 0.05$, **$p < 0.01$, ***$p < 0.001$, ****$p < 0.0001$.

(I and J) Heatmap shows the normalized fold change of glycolysis and TCA cycle metabolites in WT-MSC, db/db-MSC control siRNA, and db/db-MSC-GPC3 siRNA.

(K) Schematic showing significantly changed Glycolysis and TCA cycle metabolites. $n = 3$; Data are displayed as mean ± SEM. Significance was determined by one-way ANOVA. *: $p < 0.05$, **: $p < 0.01$.

A

Protein Group	Protein ID	Accession	Coverage (%)	#Peptides	#Unique
1	1	P20152|VIME_MOUSE	38	16	16
4	10	P02535|K1C10_MOUSE	18	8	5
6	9	Q8VDD5|MYH9_MOUSE	2	3	3
38	51	Q8BTM8|FLNA_MOUSE	1	2	2
76	94	P62806|H4_MOUSE	17	2	2
10	26	P08730|K1C13_MOUSE	9	4	2
3	2	P01872|IGHM_MOUSE	17	6	6
32	23	P10107|ANXA1_MOUSE	11	3	3
49	75	P17742|PPIA_MOUSE	12	2	2
2	3	P63260|ACTG_MOUSE	39	10	4
2	4	P60710|ACTB_MOUSE	39	10	4
23	24	P48036|ANXA5_MOUSE	7	2	2
16	34	P07356|ANXA2_MOUSE	13	3	3
8	11	P52480|KPYM_MOUSE	9	4	4

B

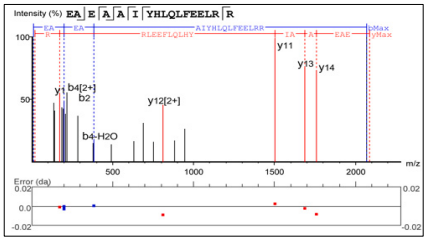

C

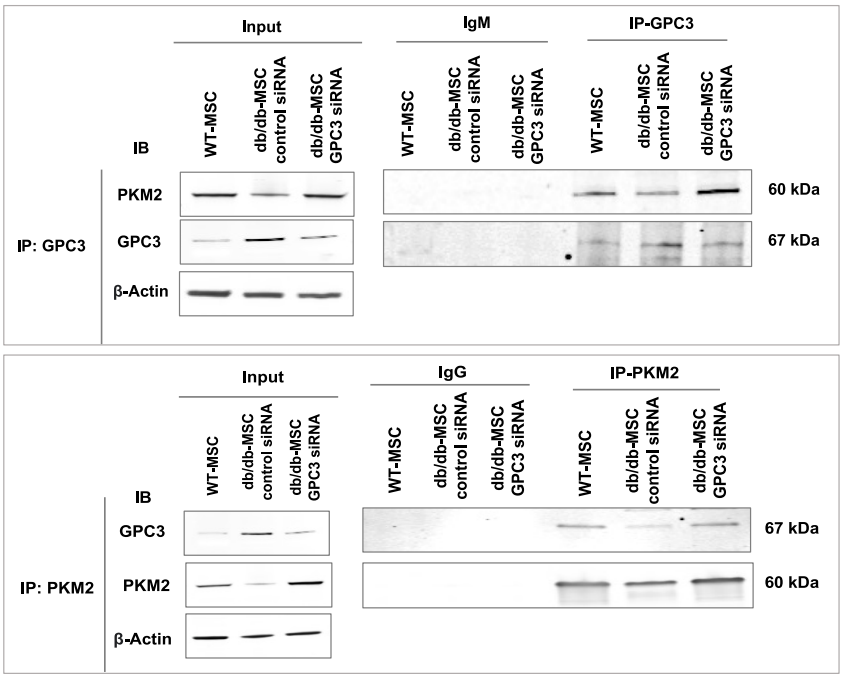

D

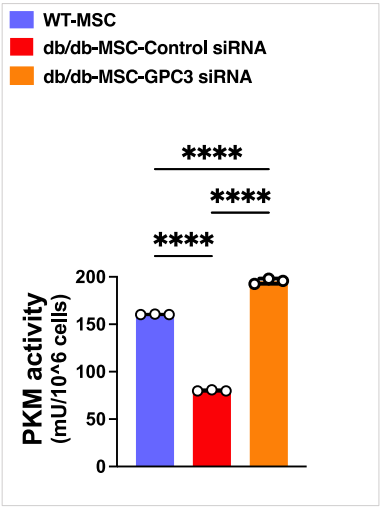

E

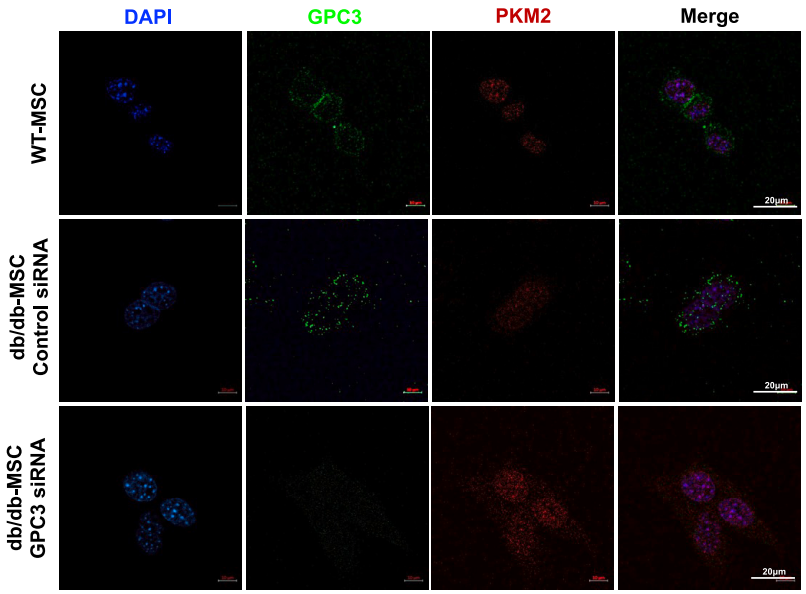

Figure 6. GPC3 directly binds with pyruvate kinase M2 (PKM2)

(A) Table showing the label-free quantified interacting proteins identified by GPC3 pull-down and proteomic analysis from the cell lysate of WT-MSC, db/db-MSC control siRNA, and db/db-MSC-GPC3 siRNA.

(B) LC-MS/MS tandem mass spectrum for the peptide sequence similar to pyruvate kinase M2 protein identification.

(C) Western blot analysis of the Co-IP complex confirmed that GPC3 interacted with PKM2 in WT-MSC, db/db-MSC control siRNA, and db/db-MSC-GPC3 siRNA. $n = 3$.

(D) Pyruvate kinase activity was determined by using ELISA. $n = 3$; Data are displayed as mean ± SEM. One-way ANOVA was used with multiple comparisons. ****$p < 0.0001$.

(E) The immunofluorescence staining was carried out to check the co-localization of GPC3 with PKM2. Scale bars: 20 μm.

To investigate the effect of GPC3-metabolic reprogrammed db/db-MSC on cardiac fibrosis, Masson's trichrome staining of cardiac tissue was performed. The results showed reduced fibrosis (Figure 7C) in post-MI hearts injected with GPC3-metabolic reprogrammed db/db-MSC compared to control-siRNA-db/db-MSC. MSCs promote cardiac repair in models of cardiac injury mainly through indirect paracrine signaling, primarily through the release of angiogenesis factors. As neovascularization/angiogenesis are essential for cardiac repair post-MI, we performed an evaluation of vessel density in the border zone of the infarct by CD31 staining and found that CD31 positive vessels were significantly increased in GPC3-metabolic reprogrammed db/db-MSC treated mice compared with control-siRNA-db/db-MSC treated mice (Figure 7D).

To assess the impact of GPC3-metabolic reprogrammed db/db-MSC on cardiac inflammation, we analyzed the expression of pro-inflammatory cytokines in the cardiac tissue on day 28. Intriguingly, RT-PCR results showed that intramyocardial injection of GPC3-metabolic reprogrammed db/db-MSC in MI heart significantly increased the mRNA expression of immunomodulatory proteins and lowered the expression of pro-inflammatory proteins compared to control-siRNA-db/db-MSC (Figures S6A and S6B). We also evaluated $CD206^{hi}$ M2-like cells and $CD68^{hi}$ cells in the border zone of the infarct. We found significantly higher numbers of $CD206^{hi}$ M2-like cells and a lower number of $CD68^{hi}$ cells in the post-MI peri-infarct area of hearts of mice injected with GPC3-metabolic reprogrammed db/db-MSC compared to control-siRNA-db/db-MSC (Figures S6C and S6D). These data suggest that GPC3-metabolic reprogrammed db/db-MSC improves angiogenic and immunomodulation ability in the myocardium and attenuates MI-induced fibrosis and LV dysfunction.

DISCUSSION

This study documents that GPC3 metabolically reprograms diabetic-MSC into a dysfunctional state and that GPC3 knockdown restores diabetic MSC functional and reparative activities. The principal findings are as follows: (1) we show that diabetic-MSC does not cf. cardiac benefit post-MI. (2) Metabolomics study revealed that diabetic-MSC has defective energy metabolism status. (3) GPC3, a heparan sulfate proteoglycan, considerably increased in diabetic-MSC and negatively influenced MSC functions and metabolic rates *in vitro*. (4) GPC3-knockdown mediated metabolic reprogramming of diabetic-MSC enhanced their functions and metabolic demands by activating pyruvate kinase M2. Collectively, GPC3 metabolic reprogramming rejuvenates the functions and metabolic status of db/db-MSC and bolsters its therapeutic efficiency in treating MI.

Cardiovascular disease (CVD) is a life-threatening problem all around the world.[45] CVD-associated mortality increases with diabetes.[2] Over the past decades, stem cell-based therapy has been used as an innovative therapeutic strategy for CVD.[46] MSC offers several advantages for cell-based treatments, including easy isolation, expansion *in vitro*, and the ability to use autologous cellular sources with a high quantity of available samples.[7] However, preclinical and clinical studies showed the advantages of allogenic MSCs application in heart failure and diabetes; its long-term efficacy is limited because of the survival of transplanted MSCs and its secretion of paracrine molecules is severely impaired as increased ROS production under hyperglycemia condition and myocardial infarction could trigger cell apoptosis.[13] By utilizing autologous MSC, we can enhance the therapeutic efficacy of cells and strengthen their ability to safeguard against limitations. Nevertheless, multiple studies have shown that metabolic diseases like diabetes and obesity have deleterious effects on the functionality of MSC.[35,47,48] In a recent study, Yu et al., showed that adipose tissue-derived-MSC isolated from subcutaneous fat of obese human subjects are less effective in repairing global and regional cardiac functions and regional deformation in hypersensitive mice.[49] In another study, the transplantation of autologous MSCs from elderly donor after MI in rats has shown reduced potential for cardiac repair compared with younger donor-derived MSC.[50] However, the effect of diabetic MSC on cardiac functions in MI is unknown. In the current study, our data demonstrated that transplantation of diabetic MSC fails to improve cardiac repair and LV functions in a mouse model of MI. Collectively, diabetic-MSC loses cardiac repair capabilities.

Glucose is the primary source of ATP for mammalian cells and can be metabolized through either oxidative phosphorylation or glycolysis. The functions of MSC are dependent on their cellular metabolic and bioenergetic state.[38,51] Limited reports investigated the metabolic activity of diabetic-MSC and the molecular mechanisms of altered metabolism that hinder their reparative activities. Employing seahorse metabolic flux assay and metabolomics studies, we observed a distinct metabolic signature of diabetic-MSC characterized by a lower rate of glycolysis, oxidative phosphorylation, and decreased production of ATP, suggesting the presence of a diminished energy metabolism state. These data corroborate recent findings from *Nguyen* et al., demonstrated that diabetic MSC from diabetic donors showed declined glycolysis, reduced mitochondria respiration, and ATP generation.[52]

Is it possible to restore the diabetes-induced diminished energy metabolism state and improve MSC cardiac reparative activities by metabolic reprogramming diabetic-MSC? Our data presented in the current study demonstrated that GPC3 knockdown in

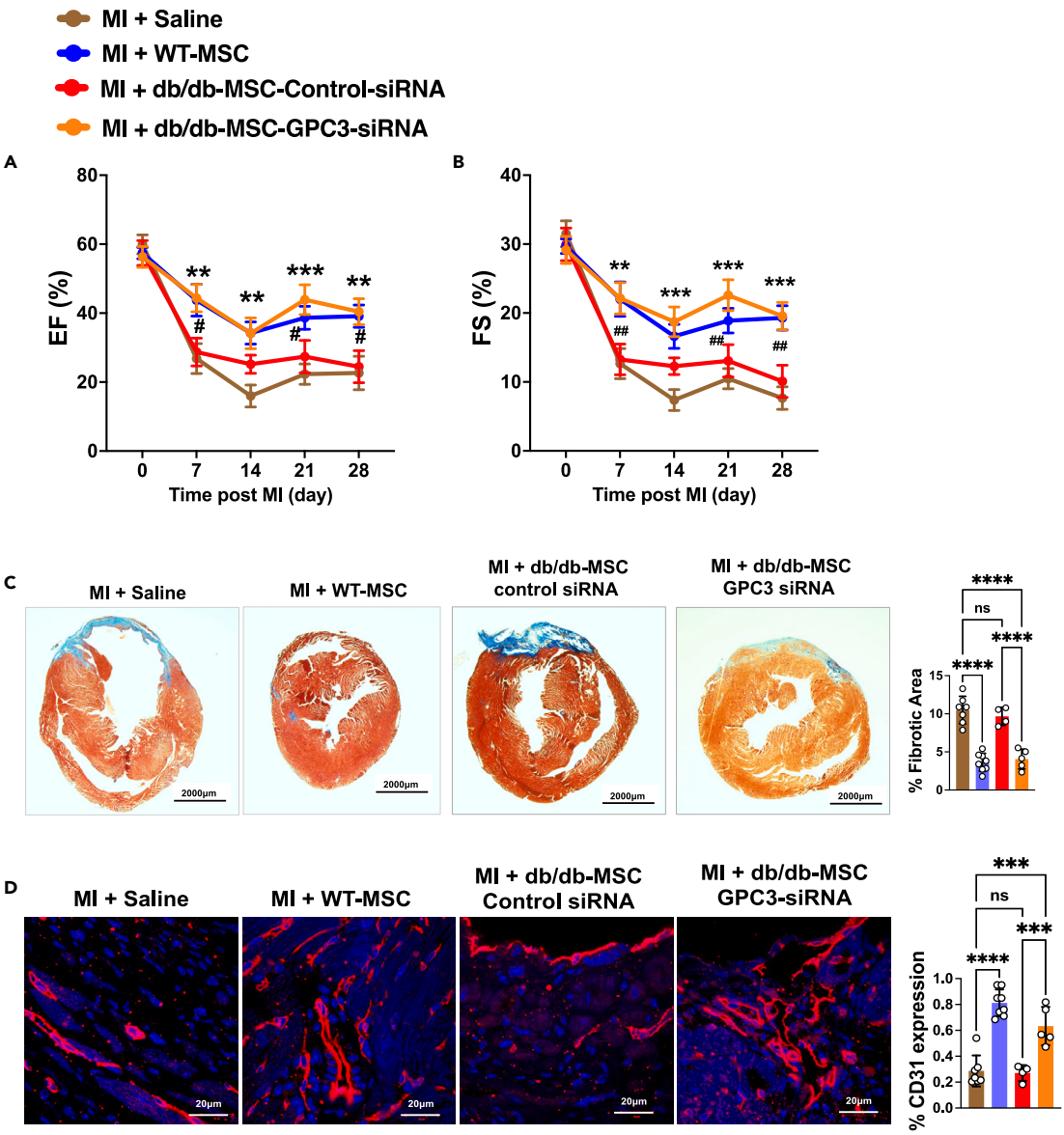

Figure 7. Intracardiac transplantation of GPC3-knockdown-db/db-MSC confers cardiac benefit post-MI

(A and B) Baseline echocardiography measurements were conducted on C57BL/6J mice and underwent left anterior descending coronary artery ligation followed by saline, WT-MSC, db/db-MSC-control siRNA, and db/db-MSC-GPC3 siRNA treatment. (A) Ejection fraction (EF) and (B) fraction shortening (FS) were assessed up to 28 days post-MI. n = 6–9/group; Data are displayed as mean ± SEM. Two-way ANOVA, in conjunction with Tukey's multiple comparisons test. $^{**}p < 0.01$, $^{***}p < 0.001$, MI + db/db-MSC-GPC3 siRNA vs. MI + saline. $^{\#}p < 0.05$, $^{\#\#}p < 0.01$, MI + db/db-MSC-GPC3 siRNA vs. MI + db/db-MSC-control siRNA.

(C) Representative images of Masson's trichrome-stained hearts at day 28 post-MI and quantification of fibrotic area. n = 4–7/group; scale bar = 1,000 μm. Data are displayed as mean ± SEM. Significance was determined by one-way ANOVA. $^{****}p < 0.0001$.

(D) Representative images of left ventricular cross-sections (infarct border zone) at day 28 post-MI immunolabeled with CD31 (red) and nuclei, DAPI (blue), and quantification of CD31 expression. n = 4–7/group; scale bar = 20 μm. Data are displayed as mean ± SEM. Significance was determined by one-way ANOVA. $^{***}p < 0.001$, $^{****}p < 0.0001$.

diabetic-MSC showed a significant improvement in metabolic state and metabolic phenotypes, which further improves immunomodulation and angiogenic potential *in vitro* and restoration of their cardiac repair activity in post-MI model, *in vivo*. GPC3, a member of the heparan sulfate proteoglycan family, functions as an oncofetal glycoprotein that is attached to the cell membrane via glycosylphosphatidylinositol (GPI).[53,54] GPC3 is reported to play a vital role in the formation and development of embryonic and fetal tissues and organs, mainly playing a negative regulatory role in preventing excessive growth of tissues and organs.[55] Its amino-terminal is a soluble protein, which can be secreted into the peripheral blood.[55] Additionally, the abnormal expression of GPC3 in adults is closely related to the occurrence and

development of various tumors.[27–29] In our study, we showed that GPC3 knockdown in db/db-MSC has a significantly increased immunosuppressive activity and angiogenesis potential Further, GPC3 knockdown in db/db-MSC significantly increased the rate of glycolysis and oxidative phosphorylation. Metabolomics analysis showed a significant reduction of the glycolysis and TCA cycle metabolites in db/db-MSC, whereas these metabolites were significantly increased in GPC3 knockdown-db/db-MSC. Recent studies showed that GPC3 knockdown decreased the cell viability, stemness, as well as glycolysis development in the hypoxia-treated hepatocellular carcinoma (HCC) cells.[55] Further, this study revealed that GPC3 knockdown decreased the global lactylation and c-myc lactylation in the hypoxia-treated HCC cells, which further decreased the c-myc protein stability and expression. In another study, Yao et al. reported that GPC3 enhances the glycolysis of liver cancer (LC) cells by upregulating the glycolytic genes Glut1, HK2, and LDH-A.[56] They also showed that HIF-1α was involved in both GPC3-regulated upregulation of glycolytic genes of HK2, PKM2, and Glut1 and downregulation of mitochondrial biogenesis regulator PGC-1α in LC cells. Further, they demonstrated that the reprogramming of glucose metabolism regulated by GPC3 plays a critical role in the growth and metastasis of LC cells.

One striking finding was that GPC3 directly binds with PKM2, which is a master immune regulator and established metabolic enzyme.[57] PKM2 plays an important role in regulating osteogenic and adipogenic differentiation of bone marrow-MSC.[58] Herein, we found that GPC3 interacts with PKM2 in db/db-MSC. Interestingly, the activity was increased in GPC3 knockdown-db/db-MSC compared to control-siRNA-db/db-MSC. Previous studies revealed that GPC3 binds to GLUT1 and decreases glucose transport activity in hepatocellular carcinoma cells.[59] PKM2 regulates cell proliferation by modulating the intercellular concentration of ATP and PEP as a tap of glucose metabolism.[60,61] PKM2 is regarded as a rate-limiting enzyme during glycolysis that catalyzes the transfer of phosphate groups from phosphoenolpyruvate to ADP and produces pyruvate in the cytoplasm.[61] Our metabolomics results showed decreased fold change in pyruvic acid and lactic acid in control-siRNA-db/db-MSC. Interestingly, GPC3 knockdown-db/db-MSC showed increased fold change in pyruvic acid and lactic acid, which are the key metabolites of glycolysis.

In summary, these data provide insights into understanding the metabolic fingerprints and molecular basis of diabetes-induced MSC dysfunction, and also confirm that GPC3 metabolic reprogramming in db/db-MSC enhances their immunosuppressive activity, angiogenic potential, and energy metabolic rates. Furthermore, our data demonstrated the preclinical therapeutic potential of GPC3 metabolic reprogrammed-db/db-MSC in treating MI and potentially other ischemic tissues.

Limitations of the study

Our study also presents certain limitations. First, we exclusively investigated GPC3 in db/db-MSC. Further research is imperative to elucidate the composition of heparan sulfate chains attached to GPC3 and their role in GPC3's functional activity. Second, although the study discovers the reprogramming of metabolic status in db/db-MSC by inhibiting GPC3, primarily mediated by PKM2, the specific mechanism through which this pathway restores the functions of GPC3 knockdown-db/db-MSC remains unclear. Third, testing the therapeutic efficiency of GPC5-modified human diabetic-MSC (human ortholog of GPC3) in the athymic nude mice model of MI is essential for verifying our discoveries. Next, to assess cardiac function in the MI-mouse model, using MRI would have provided more information. Similarly, hemodynamic assessments at the endpoint would have added further value to cardiac function. Further investigation involving MI models of large animals is necessary to fully evaluate the cardiac reparative activities of GPC3-metabolic reprogrammed-db/db-MSC.

RESOURCE AVAILABILITY

Lead contact

Further information and requests for resources and reagents should be directed to and will be fulfilled by the lead contact, Dr. Raj Kishore (raj.kishore@temple.edu).

Materials availability

New, unique materials were not generated in the course of this study.

Data and code availability

- Metabolomics data have been deposited at MassIVE with the identifier MassIVE: MSV000095670.
- The mass spectrometry proteomics data have been deposited to the ProteomeXchange Consortium via the PRIDE partner repository with the dataset identifier PXD055228.
- This paper does not report the original code.
- Additional information required to reanalyze the data reported in this paper is available from the lead contact upon request.

ACKNOWLEDGMENTS

This research was funded, in part, by National Institutes of Health grants, HL143892, HL134608, and HL147841, HL169405 (to R.K.). D.J. is supported by the American Heart Association Career Development Award 23CDA1048319.

AUTHOR CONTRIBUTIONS

D.J. and R.K. designed the study. D.J. conceptualized this study, performed experiments, and analyzed data. C.T. conceptualized parts of this study, designed and performed experiments, analyzed data, and helped in the revision of the manuscript. V.M., A.M., M.C., C.G., M.T., A.G., and C.B. performed experiments.

Mass spectrometry was performed by J.T., and M.S. W.K. assisted in data interpretation. D.J. and R.K. wrote and revised the MS and approved the final manuscript. All authors discussed the results and commented on the manuscript.

DECLARATION OF INTERESTS

The authors declare no competing of interests.

STAR★METHODS

Detailed methods are provided in the online version of this paper and include the following:

- KEY RESOURCES TABLE
- EXPERIMENTAL MODEL AND STUDY PARTICIPANT DETAILS
  - Mice
- METHOD DETAILS
  - Primary MSCs culture
  - Generation of MSC lines with stable knockdown and overexpression of GPC3
  - RNA extraction, reverse transcription, and RT-PCR
  - Western blot analysis
  - Immunofluorescence
  - Invitro cytokine stimulation and profiling of paracrine factor
  - T-cell immunosuppression assay
  - Tube formation assay
  - Metabolic flux assay
  - Metabolomics
- QUANTIFICATION AND STATISTICAL ANALYSIS

SUPPLEMENTAL INFORMATION

Supplemental information can be found online at https://doi.org/10.1016/j.isci.2024.111021.

Received: May 3, 2024
Revised: August 2, 2024
Accepted: September 20, 2024
Published: September 24, 2024

REFERENCES

1. Drucker, D.J. (2024). Prevention of cardiorenal complications in people with type 2 diabetes and obesity. Cell Metabol. *36*, 338–353. https://doi.org/10.1016/j.cmet.2023.12.018.
2. Huang, G., Cheng, Z., Hildebrand, A., Wang, C., Cimini, M., Roy, R., Lucchese, A.M., Benedict, C., Mallaredy, V., Magadum, A., et al. (2022). Diabetes impairs cardioprotective function of endothelial progenitor cell-derived extracellular vesicles via H3K9Ac inhibition. Theranostics *12*, 4415–4430. https://doi.org/10.7150/thno.70821.
3. Dal Canto, E., Ceriello, A., Rydén, L., Ferrini, M., Hansen, T.B., Schnell, O., Standl, E., and Beulens, J.W. (2019). Diabetes as a cardiovascular risk factor: An overview of global trends of macro and micro vascular complications. Eur J Prev Cardiol. *26*, 25–32. https://doi.org/10.1177/2047487319878371.
4. Yan, W., Xia, Y., Zhao, H., Xu, X., Ma, X., and Tao, L. (2024). Stem cell-based therapy in cardiac repair after myocardial infarction: Promise, challenges, and future directions. J. Mol. Cell. Cardiol. *188*, 1–14. https://doi.org/10.1016/j.yjmcc.2023.12.009.
5. Hoang, D.M., Pham, P.T., Bach, T.Q., Ngo, A.T.L., Nguyen, Q.T., Phan, T.T.K., Nguyen, G.H., Le, P.T.T., Hoang, V.T., Forsyth, N.R., et al. (2022). Stem cell-based therapy for human diseases. Signal Transduct. Targeted Ther. *7*, 272. https://doi.org/10.1038/s41392-022-01134-4.
6. Joladarashi, D., Garikipati, V.N.S., Thandavarayan, R.A., Verma, S.K., Mackie, A.R., Khan, M., Gumpert, A.M., Bhimaraj, A., Youker, K.A., Uribe, C., et al. (2015). Enhanced Cardiac Regenerative Ability of Stem Cells After Ischemia-Reperfusion Injury: Role of Human CD34+ Cells Deficient in MicroRNA-377. J. Am. Coll. Cardiol. *66*, 2214–2226. https://doi.org/10.1016/j.jacc.2015.09.009.
7. Iqbal, F., Johnston, A., Wyse, B., Rabani, R., Mander, P., Hoseini, B., Wu, J., Li, R.K., Gauthier-Fisher, A., Szaraz, P., and Librach, C. (2023). Combination human umbilical cord perivascular and endothelial colony forming cell therapy for ischemic cardiac injury. NPJ Regen. Med. *8*, 45. https://doi.org/10.1038/s41536-023-00321-3.
8. Guo, Y., Yu, Y., Hu, S., Chen, Y., and Shen, Z. (2020). The therapeutic potential of mesenchymal stem cells for cardiovascular diseases. Cell Death Dis. *11*, 349. https://doi.org/10.1038/s41419-020-2542-9.
9. Kumar, M.A., Baba, S.K., Sadida, H.Q., Marzooqi, S.A., Jerobin, J., Altemani, F.H., Algehainy, N., Alanazi, M.A., Abou-Samra, A.B., Kumar, R., et al. (2024). Extracellular vesicles as tools and targets in therapy for diseases. Signal Transduct. Targeted Ther. *9*, 27. https://doi.org/10.1038/s41392-024-01735-1.
10. Fijany, A., Sayadi, L.R., Khoshab, N., Banyard, D.A., Shaterian, A., Alexander, M., Lakey, J.R.T., Paydar, K.Z., Evans, G.R.D., and Widgerow, A.D. (2019). Mesenchymal stem cell dysfunction in diabetes. Mol. Biol. Rep. *46*, 1459–1475. https://doi.org/10.1007/s11033-018-4516-x.
11. van de Vyver, M., Niesler, C., Myburgh, K.H., and Ferris, W.F. (2016). Delayed wound healing and dysregulation of IL6/STAT3 signalling in MSCs derived from pre-diabetic obese mice. Mol. Cell. Endocrinol. *426*, 1–10. https://doi.org/10.1016/j.mce.2016.02.003.
12. Ribot, J., Denoeud, C., Frescaline, G., Landon, R., Petite, H., Pavon-Djavid, G., Bensidhoum, M., and Anagnostou, F. (2021). Experimental Type 2 Diabetes Differently Impacts on the Select Functions of Bone Marrow-Derived Multipotent Stromal Cells. Cells *10*, 268. https://doi.org/10.3390/cells10020268.
13. Qi, Y., Ma, J., Li, S., and Liu, W. (2019). Applicability of adipose-derived mesenchymal stem cells in treatment of patients with type 2 diabetes. Stem Cell Res. Ther. *10*, 274. https://doi.org/10.1186/s13287-019-1362-2.
14. Macrin, D., Alghadeer, A., Zhao, Y.T., Miklas, J.W., Hussein, A.M., Detraux, D., Robitaille, A.M., Madan, A., Moon, R.T., Wang, Y., et al. (2019). Metabolism as an early predictor of DPSCs aging. Sci. Rep. *9*, 2195. https://doi.org/10.1038/s41598-018-37489-4.
15. Li, H., Dai, H., and Li, J. (2023). Immunomodulatory properties of mesenchymal stromal/stem cells: The link with metabolism. J. Adv. Res. *45*, 15–29. https://doi.org/10.1016/j.jare.2022.05.012.
16. Ito, K., and Suda, T. (2014). Metabolic requirements for the maintenance of self-renewing stem cells. Nat. Rev. Mol. Cell Biol. *15*, 243–256. https://doi.org/10.1038/nrm3772.

17. Mastrangelo, A., Panadero, M.I., Pérez, L.M., Gálvez, B.G., García, A., Barbas, C., and Rupérez, F.J. (2016). New insight on obesity and adipose-derived stem cells using comprehensive metabolomics. Biochem. J. *473*, 2187–2203. https://doi.org/10.1042/BCJ20160241.
18. Sun, Y., Yu, X., Gao, X., Zhang, C., Sun, H., Xu, K., Wei, D., Wang, Q., Zhang, H., Shi, Y., et al. (2022). RNA sequencing profiles reveal dynamic signaling and glucose metabolic features during bone marrow mesenchymal stem cell senescence. Cell Biosci. *12*, 62. https://doi.org/10.1186/s13578-022-00796-5.
19. Patra, T., Cunningham, D.M., Meyer, K., Toth, K., Ray, R.B., Heczey, A., and Ray, R. (2023). Targeting Lin28 axis enhances glypican-3-CAR T cell efficacy against hepatic tumor initiating cell population. Mol. Ther. *31*, 715–728. https://doi.org/10.1016/j.ymthe.2023.01.002.
20. Quach, N.D., Kaur, S.P., Eggert, M.W., Ingram, L., Ghosh, D., Sheth, S., Nagy, T., Dawson, M.R., Arnold, R.D., and Cummings, B.S. (2019). Paradoxical Role of Glypican-1 in Prostate Cancer Cell and Tumor Growth. Sci. Rep. *9*, 11478. https://doi.org/10.1038/s41598-019-47874-2.
21. Filmus, J., and Selleck, S.B. (2001). Glypicans: proteoglycans with a surprise. J. Clin. Invest. *108*, 497–501. https://doi.org/10.1172/JCI13712.
22. Schepers, E.J., Glaser, K., Zwolshen, H.M., Hartman, S.J., and Bondoc, A.J. (2023). Structural and Functional Impact of Posttranslational Modification of Glypican-3 on Liver Carcinogenesis. Cancer Res. *83*, 1933–1940. https://doi.org/10.1158/0008-5472.CAN-22-3895.
23. Akkermans, O., Delloye-Bourgeois, C., Peregrina, C., Carrasquero-Ordaz, M., Kokolaki, M., Berbeira-Santana, M., Chavent, M., Reynaud, F., Raj, R., Agirre, J., et al. (2022). GPC3-Unc5 receptor complex structure and role in cell migration. Cell *185*, 3931–3949.e26. https://doi.org/10.1016/j.cell.2022.09.025.
24. Filmus, J. (2023). Glypicans, 35 years later. Proteoglycan Res. *1*, e5. https://doi.org/10.1002/pgr2.5.
25. Grisaru, S., Cano-Gauci, D., Tee, J., Filmus, J., and Rosenblum, N.D. (2001). Glypican-3 modulates BMP- and FGF-mediated effects during renal branching morphogenesis. Dev. Biol. *231*, 31–46. https://doi.org/10.1006/DBIO.2000.0127.
26. Capurro, M.I., Xu, P., Shi, W., Li, F., Jia, A., and Filmus, J. (2008). Glypican-3 Inhibits Hedgehog Signaling during Development by Competing with Patched for Hedgehog Binding. Dev. Cell *14*, 700–711. https://doi.org/10.1016/J.DEVCEL.2008.03.006.
27. Filmus, J., and Capurro, M. (2013). Glypican-3: a marker and a therapeutic target in hepatocellular carcinoma. FEBS J. *280*, 2471–2476. https://doi.org/10.1111/febs.12126.
28. Capurro, M., Wanless, I.R., Sherman, M., Deboer, G., Shi, W., Miyoshi, E., and Filmus, J. (2003). Glypican-3: a novel serum and histochemical marker for hepatocellular carcinoma. Gastroenterology *125*, 89–97. https://doi.org/10.1016/s0016-5085(03)00689-9.
29. Castillo, L.F., Tascón, R., Lago Huvelle, M.A., Novack, G., Llorens, M.C., Dos Santos, A.F., Shortrede, J., Cabanillas, A.M., Bal de Kier Joffé, E., Labriola, L., and Peters, M.G. (2016). Glypican-3 induces a mesenchymal to epithelial transition in human breast cancer cells. Oncotarget *7*, 60133–60154. https://doi.org/10.18632/oncotarget.11107.
30. Szoor, A., Vaidya, A., Velasquez, M.P., Mei, Z., Galvan, D.L., Torres, D., Gee, A., Heczey, A., and Gottschalk, S. (2017). T Cell-Activating Mesenchymal Stem Cells as a Biotherapeutic for HCC. Mol. Ther. Oncolytics *6*, 69–79. https://doi.org/10.1016/j.omto.2017.07.002.
31. Qiu, H., Shi, S., Yue, J., Xin, M., Nairn, A.V., Lin, L., Liu, X., Li, G., Archer-Hartmann, S.A., Dela Rosa, M., et al. (2018). A mutant-cell library for systematic analysis of heparan sulfate structure–function relationships. Nat. Methods *15*, 889–899. https://doi.org/10.1038/s41592-018-0189-6.
32. Yue, J., Jin, W., Yang, H., Faulkner, J., Song, X., Qiu, H., Teng, M., Azadi, P., Zhang, F., Linhardt, R.J., and Wang, L. (2021). Heparan Sulfate Facilitates Spike Protein-Mediated SARS-CoV-2 Host Cell Invasion and Contributes to Increased Infection of SARS-CoV-2 G614 Mutant and in Lung Cancer. Front. Mol. Biosci. *8*, 649575. https://doi.org/10.3389/fmolb.2021.649575.
33. Zhang, Y., Wang, J., Dong, F., Li, H., and Hou, Y. (2014). The role of GPC5 in lung metastasis of salivary adenoid cystic carcinoma. Arch. Oral Biol. *59*, 1172–1182. https://doi.org/10.1016/j.archoralbio.2014.07.009.
34. Li, Y., and Yang, P. (2011). GPC5 Gene and Its Related Pathways in Lung Cancer. J. Thorac. Oncol. *6*, 2–5. https://doi.org/10.1097/JTO.0b013e3181fd6b04.
35. Mahmoud, M., Abu-Shahba, N., Azmy, O., and El-Badri, N. (2019). Impact of Diabetes Mellitus on Human Mesenchymal Stromal Cell Biology and Functionality: Implications for Autologous Transplantation. Stem Cell Rev. Rep. *15*, 194–217. https://doi.org/10.1007/s12015-018-9869-y.
36. Beegle, J., Lakatos, K., Kalomoiris, S., Stewart, H., Isseroff, R.R., Nolta, J.A., and Fierro, F.A. (2015). Hypoxic preconditioning of mesenchymal stromal cells induces metabolic changes, enhances survival, and promotes cell retention in vivo. Stem Cell. *33*, 1818–1828. https://doi.org/10.1002/stem.1976.
37. Mendt, M., Daher, M., Basar, R., Shanley, M., Kumar, B., Wei Inng, F.L., Acharya, S., Shaim, H., Fowlkes, N., Tran, J.P., et al. (2021). Metabolic Reprogramming of GMP Grade Cord Tissue Derived Mesenchymal Stem Cells Enhances Their Suppressive Potential in GVHD. Front. Immunol. *12*, 631353. https://doi.org/10.3389/fimmu.2021.631353.
38. Salazar-Noratto, G.E., Luo, G., Denoeud, C., Padrona, M., Moya, A., Bensidhoum, M., Bizios, R., Potier, E., Logeart-Avramoglou, D., and Petite, H. (2020). Understanding and leveraging cell metabolism to enhance mesenchymal stem cell transplantation survival in tissue engineering and regenerative medicine applications. Stem Cell. *38*, 22–33. https://doi.org/10.1002/stem.3079.
39. Ko, K.I., Coimbra, L.S., Tian, C., Alblowi, J., Kayal, R.A., Einhorn, T.A., Gerstenfeld, L.C., Pignolo, R.J., and Graves, D.T. (2015). Diabetes reduces mesenchymal stem cells in fracture healing through a TNFα-mediated mechanism. Diabetologia *58*, 633–642. https://doi.org/10.1007/s00125-014-3470-y.
40. Song, N., Scholtemeijer, M., and Shah, K. (2020). Mesenchymal Stem Cell Immunomodulation: Mechanisms and Therapeutic Potential. Trends Pharmacol. Sci. *41*, 653–664. https://doi.org/10.1016/j.tips.2020.06.009.
41. Bansal, S.S., Ismahil, M.A., Goel, M., Patel, B., Hamid, T., Rokosh, G., and Prabhu, S.D. (2017). Activated T lymphocytes are essential drivers of pathological remodeling in ischemic heart failure. Circ. Heart Fail. *10*, e003688. https://doi.org/10.1161/CIRCHEARTFAILURE.116.003688.
42. Marinescu, C.I., Preda, M.B., and Burlacu, A. (2021). A procedure for in vitro evaluation of the immunosuppressive effect of mouse mesenchymal stem cells on activated T cell proliferation. Stem Cell Res. Ther. *12*, 319. https://doi.org/10.1186/s13287-021-02344-3.
43. Robich, M.P., Chu, L.M., Oyamada, S., Sodha, N.R., and Sellke, F.W. (2011). Myocardial therapeutic angiogenesis: a review of the state of development and future obstacles. Expert Rev. Cardiovasc Ther. *9*, 1469–1479. https://doi.org/10.1586/erc.11.148.
44. Li, X.B., Gu, J.D., and Zhou, Q.H. (2015). Review of aerobic glycolysis and its key enzymes - new targets for lung cancer therapy. Thorac. Cancer *6*, 17–24. https://doi.org/10.1111/1759-7714.12148.
45. Tsao, C.W., Aday, A.W., Almarzooq, Z.I., Anderson, C.A.M., Arora, P., Avery, C.L., Baker-Smith, C.M., Beaton, A.Z., Boehme, A.K., Buxton, A.E., et al. (2023). Heart Disease and Stroke Statistics-2023 Update: A Report From the American Heart Association. Circulation *147*, e93–e621. https://doi.org/10.1161/CIR.0000000000001123.
46. Banerjee, M.N., Bolli, R., and Hare, J.M. (2018). Clinical studies of cell therapy in cardiovascular medicine recent developments and future directions. Circ. Res. *123*, 266–287. https://doi.org/10.1161/CIRCRESAHA.118.311217/FORMAT/EPUB.
47. Kornicka, K., Houston, J., and Marycz, K. (2018). Dysfunction of Mesenchymal Stem Cells Isolated from Metabolic Syndrome and Type 2 Diabetic Patients as Result of Oxidative Stress and Autophagy may Limit Their Potential Therapeutic Use. Stem Cell Rev. Rep. *14*, 337–345. https://doi.org/10.1007/s12015-018-9809-x.
48. Hong, S., Huang, W., Zhu, X., Tang, H., Krier, J.D., Xing, L., Lu, B., Gandhi, D., Jordan, K.L., Saadiq, I.M., et al. (2023). Obesity blunts amelioration of cardiac hypertrophy and fibrosis by human mesenchymal stem/stromal cell-derived extracellular vesicles. Am. J. Physiol. Heart Circ. Physiol. *325*, H163–H171. https://doi.org/10.1152/ajpheart.00676.2022.
49. Yu, S., Klomjit, N., Jiang, K., Zhu, X.Y., Ferguson, C.M., Conley, S.M., Obeidat, Y., Kellogg, T.A., McKenzie, T., Heimbach, J.K., et al. (2023). Human Obesity Attenuates Cardioprotection Conferred by Adipose Tissue–Derived Mesenchymal Stem/Stromal Cells. J. Cardiovasc. Transl. Res. *16*, 221–232. https://doi.org/10.1007/s12265-022-10279-0.
50. Zhu, W., Du, W., Duan, R., Liu, Y., Zong, B., Jin, X., Dong, Z., Wang, H., Shahab, S., Wang, H., et al. (2023). miR-873-5p Suppression Reinvigorates Aging Mesenchymal Stem Cells and Improves Cardiac Repair after Myocardial Infarction. ACS Pharmacol. Transl. Sci. *7*, 743–756. https://doi.org/10.1021/ACSPTSCI.3C00293/ASSET/IMAGES/MEDIUM/PT3C00293_0008.GIF.
51. Tencerova, M., Rendina-Ruedy, E., Neess, D., Færgeman, N., Figeac, F., Ali, D., Danielsen, M., Haakonsson, A., Rosen, C.J., and Kassem, M. (2019). Metabolic programming determines the lineage-differentiation fate of murine bone marrow stromal progenitor

cells. Bone Res. *7*, 35. https://doi.org/10.1038/s41413-019-0076-5.

52. Nguyen, L.T., Hoang, D.M., Nguyen, K.T., Bui, D.M., Nguyen, H.T., Le, H.T.A., Hoang, V.T., Bui, H.T.H., Dam, P.T.M., Hoang, X.T.A., et al. (2021). Type 2 diabetes mellitus duration and obesity alter the efficacy of autologously transplanted bone marrow-derived mesenchymal stem/stromal cells. Stem Cells Transl. Med. *10*, 1266–1278. https://doi.org/10.1002/sctm.20-0506.
53. Chen, C., Huang, X., Ying, Z., Wu, D., Yu, Y., Wang, X., and Chen, C. (2017). Can glypican-3 be a disease-specific biomarker? Clin. Transl. Med. *6*, 18. https://doi.org/10.1186/s40169-017-0146-5.
54. Zhao, J., Qin, L., He, G., Xie, T., Hu, G., Wang, F., Zhong, H., Zhu, J., and Xu, Y. (2023). Administration of a glypican-3 peptide increases the infiltration and cytotoxicity of CD8+ T cells against testicular yolk sac tumor, associated with enhancing the intratumoral cGAS/STING signaling. Cancer Med. *12*, 21293–21307. https://doi.org/10.1002/cam4.6605.
55. Yao, G., and Yang, Z. (2023). Glypican-3 knockdown inhibits the cell growth, stemness, and glycolysis development of hepatocellular carcinoma cells under hypoxic microenvironment through lactylation. Arch. Physiol. Biochem. *130*, 546–554. https://doi.org/10.1080/13813455.2023.2206982.
56. Yao, G., Yin, J., Wang, Q., Dong, R., and Lu, J. (2019). Glypican-3 Enhances Reprogramming of Glucose Metabolism in Liver Cancer Cells. BioMed Res. Int. *2019*, 2560650. https://doi.org/10.1155/2019/2560650.
57. Rao, J., Wang, H., Ni, M., Wang, Z., Wang, Z., Wei, S., Liu, M., Wang, P., Qiu, J., Zhang, L., et al. (2022). FSTL1 promotes liver fibrosis by reprogramming macrophage function through modulating the intracellular function of PKM2. Gut *71*, 2539–2550. https://doi.org/10.1136/gutjnl-2021-325150.
58. Puckett, D.L., Alquraishi, M., Chowanadisai, W., and Bettaieb, A. (2021). The Role of PKM2 in Metabolic Reprogramming: Insights into the Regulatory Roles of Non-Coding RNAs. Int. J. Mol. Sci. *22*, 1171. https://doi.org/10.3390/ijms22031171.
59. Cho, H.S., Ahn, J.M., Han, H.J., and Cho, J.Y. (2010). Glypican 3 binds to GLUT1 and decreases glucose transport activity in hepatocellular carcinoma cells. J. Cell. Biochem. *111*, 1252–1259. https://doi.org/10.1002/jcb.22848.
60. Zhang, Z., Deng, X., Liu, Y., Liu, Y., Sun, L., and Chen, F. (2019). PKM2, function and expression and regulation. Cell Biosci. *9*, 1–25. BioMed Central Ltd.
61. Walls, J.F., Subleski, J.J., Palmieri, E.M., Gonzalez-Cotto, M., Gardiner, C.M., McVicar, D.W., and Finlay, D.K. (2020). Metabolic but not transcriptional regulation by pkm2 is important for natural killer cell responses. eLife *9*, e59166. https://doi.org/10.7554/ELIFE.59166.
62. Yuan, X., Liu, Y., Bijonowski, B.M., Tsai, A.C., Fu, Q., Logan, T.M., Ma, T., and Li, Y. (2020). NAD^+/NADH redox alterations reconfigure metabolism and rejuvenate senescent human mesenchymal stem cells in vitro. Commun. Biol. *3*, 774. https://doi.org/10.1038/s42003-020-01514-y.
63. Garikipati, V.N.S., Krishnamurthy, P., Verma, S.K., Khan, M., Abramova, T., Mackie, A.R., Qin, G., Benedict, C., Nickoloff, E., Johnson, J., et al. (2015). Negative Regulation of miR-375 by Interleukin-10 Enhances Bone Marrow-Derived Progenitor Cell-Mediated Myocardial Repair and Function After Myocardial Infarction. Stem Cells *33*, 3519–3529. https://doi.org/10.1002/stem.2121.
64. Garikipati, V.N.S., Verma, S.K., Jolardarashi, D., Cheng, Z., Ibetti, J., Cimini, M., Tang, Y., Khan, M., Yue, Y., Benedict, C., et al. (2017). Therapeutic Inhibition of miR-375 Attenuates Post-MI Inflammatory Response and Left Ventricular Dysfunction via PDK-1-AKT Signaling Axis. Cardiovasc. Res. *113*, 938–949. https://doi.org/10.1093/cvr/cvx052.
65. Garikipati, V.N.S., Verma, S.K., Cheng, Z., Liang, D., Truongcao, M.M., Cimini, M., Yue, Y., Huang, G., Wang, C., Benedict, C., et al. (2019). Circular RNA CircFndc3b modulates cardiac repair after myocardial infarction via FUS/VEGF-A axis. Nat. Commun. *10*, 4317. https://doi.org/10.1038/s41467-019-11777-7.

STAR★METHODS

KEY RESOURCES TABLE

REAGENT or RESOURCE	SOURCE	IDENTIFIER
Antibodies		
PE Rat Anti-Mouse CD90.2 Clone 53-2.1 (RUO)	BD Biosciences	Cat# 553006; RRID: AB_394545
Alexa Fluor® 647 Rat Anti-Mouse CD105	BD Biosciences	Cat# 562761; RRID: AB_2737775
CD31	R&D Biosystems	Cat# AF3628; RRID: AB_2161028
Glypican-3 Antibody (F-3) AC	Santa Cruz Biotechnology	Cat# sc-390587 AC
Glypican-3 Antibody (F-3) Alexa Fluor® 488	Santa Cruz Biotechnology	Cat# sc-390587 AF488
CoraLite®594-conjugated PKM2-specific Monoclonal antibody	Ptoteintech	Cat# CL594-60268
Mouse MMR/CD206 antibody	R&D system	Cat# AF2535; RRID: AB_2063012
CD68 polyclonal antibody	Ptoteintech	Cat# 28058-1-AP
PKM2 (D78A4) XP® Rabbit mAb (Sepharose® Bead Conjugate)	Cell Signalling Technology	Cat# 13266; RRID: AB_2798165
PKM2 (D78A4) XP® Rabbit mAb #4053	Cell Signalling Technology	Cat# 4053; RRID: AB_1904096
GAPDH	Ptoteintech	Cat# 60004-1-Ig
β-Actin	Santa Cruz Biotechnology	Cat# sc-47778
Chemicals, peptides, and recombinant proteins		
StemPro™ Adipogenesis Differentiation Kit	Thermofisher Scientific	A1007001
StemPro™ Chondrogenesis Differentiation Kit	Thermofisher Scientific	A1007101
StemPro™ Osteogenesis Differentiation Kit	Thermofisher Scientific	A1007201
Oil Red O solution	Millipore-Sigma	O1391-250ML
Alizarin-Red Staining Solution	Millipore-Sigma	TMS-008-C
Alcian-Blue Staining Solution	Millipore-Sigma	TMS-010-C
Mouse FGF-Basic Recombinant Protein	Thermofisher Scientific	PMG0034
Dulbecco's Modified Eagle's Medium/ Nutrient Mixture F-12 Ham	Sigma	D8437
GPC3 siRNA	Applied Biological Materials Inc	224480940296
ViralEntryTM Transduction Enhancer	Applied Biological Materials Inc	G515
Scrambled siRNA GFP Lentivirus	Applied Biological Materials Inc	LVP015-G
GPC3 Lentivirus	Applied Biological Materials Inc	224480640396
Lenti-CMV-GFP-2A-Puro-Blank Lentivirus	Applied Biological Materials Inc	LVP690
Intercept® (PBS) Blocking Buffer	LI-COR	927-70001
Mitomycin C ready made solution	Millipore Sigma	M5353-0.2ML
IFN-gamma, mouse, recombinant	Promocell	D-60724
TNF-alpha, mouse, recombinant (E. coli)	Promocell	D-63720
Dynabeads™ Mouse T-Activator CD3/CD28 for T-Cell Expansion and Activation	Thermofisher scientific	11452D
Puromycin dihydrochloride	Millipore Sigma	P9620-10ML
RIPA Lysis Buffer System,	Santa Cruz	sc-24948
D-glucose (u-13c6, 99%)	Cambridge Isotope Laboratories	CLM-1396-1
Seahorse XFe96 FluxPak mini	Agilent	102601-100
Seahorse XF base medium	Agilent	103334-100
Seahorse XF 200 mM glutamine solution, 50 mL	Agilent	103579-100
Seahorse XF DMEM medium	Agilent	103575-100
Seahorse XF 1.0 M glucose solution, 50 mL	Agilent	103577-100

(*Continued on next page*)

Continued

REAGENT or RESOURCE	SOURCE	IDENTIFIER
Seahorse XF 100 mM pyruvate solution, 50 mL	Agilent	103578-100
Seahorse XF 200 mM glutamine solution, 50 mL	Agilent	103579-100
Blocking Reagent	Santa Cruz	sc-516214
Critical commercial assays		
Prostaglandin E2 Parameter Assay Kit	R&D system	KGE004B
Pan T Cell Isolation Kit II, mouse	Miltenyi Biotec	130-095-130
BrdU Cell Proliferation Assay	Millipore Sigma	QIA58-1000TEST
Seahorse XF Cell Mito Stress Test Kit	Agilent	103010-100
Seahorse XF Glycolysis Stress Test Kit	Agilent	103017-100
Pyruvate Kinase Assay Kit	Abcam	ab83432
Deposited data		
Metabolomics	This paper	MassIVE: MSV000095670
Proteomics	This paper	PRIDE: PXD055228
Experimental models: Organisms/strains		
Ten to twelve-week-old male mice (C57BL/6J)	Bar Harbor, ME	N/A
Eight to ten-week-old diabetic male mice (BKS.Cg-Dock7m +/+ Leprdb/J-homozygous)	Jackson Research Laboratory	#000642
nondiabetic mice (BKS.Cg-Dock7m +/+ Leprdb/J-heterozygous)	Jackson Research Laboratory	#000642
Oligonucleotides		
Oligonucleotides	See Tables S1 and S2	N/A
Software and algorithms		
GraphPad Prism 9	GraphPad Prism Software, Inc	https://www.graphpad.com/
Seahorse Wave v.2.2.0	Agilent	Seahorse Wave, RRID: SCR_014526
Vevo Strain	Fujifilm Visualsonics	https://www.visualsonics.com/product/software/vevo-strain-software
ImageJ 1.52h	National Institute of Health	https://imagej.nih.gov/

EXPERIMENTAL MODEL AND STUDY PARTICIPANT DETAILS

Mice

All animal procedures were performed following the approved protocols of the Institutional Animal Care and Use Committee of Temple University (IACUC protocol #4985). Ten to twelve-week-old male mice (C57BL/6J) were purchased from Jackson Research Laboratory (Bar Harbor, ME) for MI surgery. Eight to ten-week-old diabetic male mice (Strain # 000642 BKS.Cg-*Dock7*^{m} +/+ *Lepr*^{db}/J-homozygous) hereafter db/db and non-diabetic mice (Strain # 000642 BKS.Cg-*Dock7*^{m}+/+ *Lepr*^{db}/J-heterozygous) hereafter WT were purchased from Jackson Research Laboratory for mesenchymal stromal cell (MSC) isolation.

METHOD DETAILS

Primary MSCs culture

MSCs were isolated from the bone marrow of 10–12-week-old C57BL/6J WT and db/db mice as previously reported.62,63 In brief, cells were cultured in F12 medium (Sigma) containing 10% heat-inactivated FBS (Invitrogen) and antibiotics (penicillin, 100 U/ml; streptomycin, 100 μg/ml; Invitrogen) at 37°C and 5% CO2 in a humidified chamber until confluent. The adherent cells were then dissociated with 0.25% trypsin containing 0.02% EDTA (Gibco) for 3-5 passages. MSCs were characterized and confirmed by flow cytometry using PE-conjugated CD90 (Biosciences), AF647-conjugated CD105 (Biosciences), and FITC-conjugated CD45 (Biosciences). MSCs were further characterized by their differentiation potential using the adipogenic (Thermofisher scientific), osteogenic (Thermofisher scientific), and chondrogenic (Thermofisher scientific), differentiation kit according to manufacturer's instructions. At the end of 21 days, the cells were fixed and stained with oil red O (adipogenesis), alizarin red (osteogenesis), and alcian blue (chondrogenesis), respectively.

Generation of MSC lines with stable knockdown and overexpression of GPC3

GPC3-siRNA (Figure 4A), GPC3 lentivirus (Figure S3A), and respective negative control plasmids were transduced into MSCs (Applied Biological Materials Inc). Stably transfected cell lines were obtained in a culture medium containing puromycin (4 μg/ml). The culture medium was changed every 2 days. The selection was performed for about 1 week. GPC3 expression in transfected cell lines was examined by western blotting. To detect transfection efficiency, the vectors carried the green fluorescent protein gene.

RNA extraction, reverse transcription, and RT-PCR

RNA was isolated from cells and tissues using miRNeasy Mini kit (Qiagen). NanoDrop-1000 (Thermo Scientific) was used to measure RNA concentration and purity determined by the 260A/280A ratio. A high-capacity cDNA Reverse Transcription Kit (Applied Biosystems) was used to obtain cDNA. RT-PCR was performed on an Applied Biosystems 770 StepOnePlus system using the Fast SYBR™ Green Master Mix (Applied ThermoFisher) according to the manufacturer's instructions. Fold changes were normalized to GAPDH using the threshold delta-delta cycle method. The list of primers used in the study is shown in supplement Tables S1 and S2.

Western blot analysis

Protein lysate was extracted from cells using ice-cold radio immunoprecipitation assay (RIPA) buffer [158mM NaCl, 10mM Tris HCl, pH 7.2, 1mM ethylene glycol tetra-acetic acid (EGTA), 1 mM sodium orthovanadate, 0.1% SDS, 1.0% Triton X-100, 1% Sodium deoxycholate, 1mM phenylmethylsulfonyl fluoride] 5. BCA protein assay (Fisher Scientific) was used to determine total protein lysate concentration as per the manufacturer's protocol, and 50 μg of protein lysate was electrophoresed and analyzed using primary antibodies. Equal protein loading in each lane was normalized using antibodies against housekeeping genes such as GAPDH and β-actin. The antibodies used are listed in the key source table.

Immunofluorescence

MSCs were fixed with 4% paraformaldehyde at 37°C for 45 min and washed with TBST for 5 times. Then, the blocking solution containing 0.5% Triton X-100 and 5% FBS was used to block the cells at room temperature for 45 min in the dark. Next, the diluted primary antibody (GPC3, 1:500) was added to the cells and incubated overnight at 4°C. The next day, the cells were washed with TBST and incubated for 1 h with anti-goat or anti-rabbit Alexa Fluor 488 (1:200). Then, cells were washed 5 times and incubated with DAPI in the dark for 30 min. Finally, the cells were sealed with the film-sealing liquid containing an anti-quenching agent and observed under a fluorescence microscope.

Invitro cytokine stimulation and profiling of paracrine factor

MSCs were treated with 10 ng/mL IFN-γ and 15 ng/mL TNF-α (R&D Systems) (primed MSCs) or not (resting MSCs) for 48 hours. Condition media was collected, and the levels of different paracrine factors secreted were determined using quantibody mouse inflammation array 1 (Raybiotech Inc.) according to the manufacturer's instructions. In addition, the levels of PGE2 were determined using the prostaglandin E2 parameter assay kit (R&D systems), following the manufacturer's instructions.

T-cell immunosuppression assay

MSCs treated with Mitomycin were co-cultured with T-cells isolated from the mouse spleen using a Pan T cell isolation kit (Miltenyi Biotech). The T-cells were activated using dynabeads mouse T-cell activator CD3/CD28. Three days after the co-culture, T-cell proliferation was measured using an ELISA BrdU colorimetric kit (Roche Diagnostics) per the manufacturer's instructions.

Tube formation assay

Growth factor reduced (GFR) matrigel (Corning) was thawed at 4°C overnight on ice. Exactly 10 μl of matrigel was coated onto each inner well of the μ-angiogenesis slides (IBIDI) and solidified at 37°C for 30 min. A total of 1×10^4 HUVECs were reconstituted in CM from the different MSCs, EGM, or serum-free medium to a total volume of 50 μl and plated on the GFR matrigel. The plates were incubated for 6 h in a humidified incubator at 5% CO2 and 37°C. Images were taken using an inverted phase-contrast microscope (Nikon) under 4× and 10× objectives. The tube length was measured using WimTube (Wimasis, GmbH) from the 4× magnification images of 3 wells in each condition (4×). The experimental samples and controls were assayed in triplicates.

Metabolic flux assay

Metabolic flux analyses were performed using the Seahorse XFe96 extracellular flux analyzer (Agilent). For the Seahorse metabolic flux assay, MSCs were seeded at 40,000 cells/well of 96 well plates on Seahorse XFp cell culture mini plates (Agilent) to create a confluent monolayer. XFP flux cartridges (Agilent) were pre-hydrated in XF Calibrant (Agilent) overnight at 37°C prior to running the assay. One hour prior to measurement, the medium was replaced with Seahorse XF DMEM medium supplemented with Seahorse XF Glucose (10 mM), Pyruvate (1 mM), and L-Glutamine (2 mM) (Agilent), and cells were incubated at 37°C in an incubator without CO2 for 1 h. For ECAR measurements (Seahorse XFp Glycolysis Stress Test Kit), after baseline measurements, 10 mM glucose, 1 μM oligomycin, and 50 mM 2-deoxy d-glucose (2DG) were sequentially injected into each well. For OCR measurements (Seahorse XFp Cell mito stress test kit), the medium contained 10 mM glucose in the

presence or absence of 1 mM pyruvate. After baseline measurements, 1 μM oligomycin for MSC 3 μM FCCP, 1 μM rotenone, and 1 μM antimycin A (R/A) were sequentially injected into each well. Results were analyzed using Seahorse Wave Desktop Software (Agilent).

Metabolomics

^{13}C-glucose labeling and LC-MS analysis of MSC metabolites

13C-glucose labeling, metabolite extraction, and chemical derivatization were performed according to *Yuan* et al.[62] Briefly, glucose-free DMEM medium supplemented with a 2:3 mixture of unlabeled and U-^{13}C-labeled glucose (Cambridge Isotopes Laboratories) at the same concentration for MSC expansion (1.0 g/L glucose). Cells were seeded and cultured for 2 days in DMEM with the unlabeled medium. The culture medium was then replaced with an isotope-enriched medium and cultured for an additional 3 days. The cells were collected by washing with PBS, quenching with liquid nitrogen, and adding a solution of methanol: water (4:1) directly to the culture plate to stop metabolism and lyse the cells on dry ice, followed by the addition of the internal standard (leucine 28 μg/ml solution) and incubation at −80°C for 10 min. The extracts were centrifuged at 5000 x g for 5 min at 4°C, and the supernatants were collected and transferred to a silanized Reacti-Vial (Wheaton) and stored at −80°C. The samples were subjected to LC-MS analysis (Proteomics and Metabolomics Core Facility Weill Cornell Medicine) for metabolite identification. Bioinformatic data analysis was performed by Creative Proteomics (New York, NY, USA).

GPC3 pull down and proteomics

MSC at 80% confluence, protein lysate was isolated using RIPA Lysis Buffer System (Santa Cruz), and protein concentration was determined using Pierce BCA Protein Assay Kit (Thermo Fisher) as per manufacturer's instructions. Immunoprecipitation of GPC3 was done by incubating the GPC3 primary antibody (SCBT) with isolated proteins for 2 h at 4°C, then agarose conjugate suspension (SCBT) was added to the mixture, and it was incubated on a rotating device, overnight at 4°C. The pellet was collected by centrifugation at 3,000 rpm for 30 seconds at 4°C. Then, the pellet was washed with 1XPBS three times. After the final wash, the pellet was reconstituted in 50mM ammonium bicarbonate, followed by reduction using 5mM dithiothreitol for 30 min at 60°C. The solution was cooled down to room temperature and alkylated using 10mM iodoacetamide for 30 min at room temperature. The samples were then enzymatically digested using trypsin-LysC enzyme (Roche Applied Science) and incubated overnight at 37°C. The trypsinization was stopped with 1% formic acid, and the solution was dried by vacuum centrifugation. The dried sample was resuspended in 2% ACN/water/0.1% TFA and passed through C-18 zip tips (Thermo-Scientific); the cleaned peptides were eluted using 60% ACN/water/0.1% TFA and dried by vacuum centrifugation. The cleaned peptides were further stored at -20°C until analyzed using LC-MS/MS.

Liquid chromatography-tandem mass spectrometry (LC-MS/MS) analysis

Nano-LC-MS/MS separation was performed using a nano-Acquity UPLC (Waters Technology) and Q-Exactive mass spectrometer HF (Thermo-Fisher Scientific). Reversed phased C-18 analytical (BEH C18, 150 μm × 100 mm) and trapping (180 μm × 20 mm) columns from Waters technology were used with a 75 min method with a gradient from 2 to 98% acetonitrile in 55min, using 99% water / 1% acetonitrile/ 0.1% formic acid as mobile phase A and 99% acetonitrile/ 1% water /0.1% formic acid as mobile phase B at a flow rate of 0.5 μL/min. Data-dependent acquisition tandem MS was acquired in the positive ionization mode for the top 20 most abundant precursor ions. Full MS scans were acquired from *m/z* 350–2000 with 60,000 resolution using an automatic gain control (AGC) target of 1e^6 and a maximum IT of 100 ms. Dynamic exclusion (12 s) was enabled. The minimum intensity threshold for precursor selection was set to 1 e^4, and the minimum AGC target was set at 5 e^5. Precursor ions were fragmented using 1 micro scans at a resolution of 15,000 with a maximum injection time of 50 ms and an AGC value of 2 e^5 using higher energy collision-induced dissociation (HCD) normalized collision energy of 27.

Proteomics data analysis

The LC-MS/MS data were collected as raw data files and analyzed using PEAKS proteome software Xpro (Bioinformatics Solutions, Inc.) against the UniProt/SwissPro database with a precursor mass tolerance of 10 ppm and MS/MS of 0.02 Da. Trypsin/LysC were selected as the enzyme with up to three missed cleavages. Carbamidomethylation modifications were selected as a fixed modification. Peptide identification was performed at a 1% false discovery rate. A peaksPTM search was queued after the peaksDB search, using advanced settings of a larger set of variable modifications, including hydroxyprolination, oxidation M, hydroxylation K, hydroxylation-Hex K, hydroxylation-Hex-Hex K, HexNAc ST, HexHexNAc ST, phosphorylation STY, ubiquitination K, acetylation and deamidation N. The final protein list generated was a combination of peaksDB and peaksPTM searches. The label-free quantification was achieved using PEAKS Studio Quantification- a label-free module with a setting of mass error tolerance of 20 ppm and a retention time shift tolerance of 2.0 min, and all abundances were normalized using total ion chromatograms (TICs).

Myocardial infarction and study design

Mice were anesthetized with 2% isoflurane inhalation with an isoflurane delivery system (Viking Medical) and were subjected to MI by ligation of the left anterior descending coronary artery (LAD) as described previously.[2,63–65] Immediately after LAD ligation, mice received an intramyocardial injection of 5x10^5 WT-MSC or db/db-MSC control-siRNA or db/db-MSC GPC3-siRNA or saline in a total volume of 20 μl at 3

different sites (basal anterior, mid anterior and apical anterior) in the peri-infarct area. Cardiac function was examined on days 0, 7, 14, and 28 using echocardiography, and morphological analyses were performed 28 days post-MI.

Echocardiography

Transthoracic two-dimensional M-mode echocardiography using the Vevo2100 equipped with 30 MHz transducers (Visual Sonics) was performed before MI (baseline) and 7-, 14-, and 28 days after surgery as described previously.[2,63–65] Mice were anesthetized with a mixture of 1.5% isoflurane and oxygen (1 L/min) with an isoflurane delivery system (Viking Medical). The internal diameter of the LV was measured in the short-axis view from M-mode recordings; percent ejection fraction (% EF) and fractional shortening (% FS) were calculated using corresponding formulas as previously described.

Tissue preparation and immunohistochemistry

Mouse heart tissue samples were fixed in 10% formalin for at least 48 hours and embedded in paraffin. Cardiac tissues were cross-sectioned into 4-5μm thick slides. Masson Trichrome staining (Sigma Aldrich) was performed following the manufacturer's instructions. CD31 identification was performed using AF3628 from R&D Systems. Images were acquired using the Eclipse Ti fluorescence microscope (Nikon) using 20× objective and planimetry analysis using ImageJ.

QUANTIFICATION AND STATISTICAL ANALYSIS

Statistical analyses were performed using GraphPad Prism 9.0 software (GraphPad). Data are expressed and plotted as the Mean ± SEM or Mean ± SD as indicated in figure legends and results. The sample size used in each experiment is indicated in the figure legends. An unpaired t-test was used to compare 2 sample groups. For comparisons of more than two groups, one-way ANOVA was done with a Tukey Posthoc test followed by Dunn's pairwise comparisons. Two-way ANOVA with Tukey's multiple comparisons test was used for echocardiography parameters with repeated measures over time. Significant differences are indicated as follows: *$p < 0.05$, **$p < 0.01$, ***$p < 0.001$, ****$p < 0.0001$.